

DESIGN, MODELING, AND EXPERIMENT OF A PIEZOELECTRIC PRESSURE SENSOR BASED
ON A THICKNESS-SHEAR MODE CRYSTAL RESONATOR

Thanh Tuong Pham

Thesis Prepared for the Degree of
MASTER OF SCIENCE

UNIVERSITY OF NORTH TEXAS

May 2017

APPROVED:

Haifeing Zhang, Major Professor
Phillip R. Foster, Committee Member
Shuping Wang, Committee Member
Enrique Barbieri, Chair of the Department of
Engineering Technology
Costas Tsatsoulis, Dean of the College of
Engineering
Victor Prybutok, Vice Provost of the Toulouse
Graduate School

Pham, Thanh Tuong. *Design, Modeling, and Experiment of a Piezoelectric Pressure Sensor based on a Thickness-Shear Mode Crystal Resonator*. Master of Science (Engineering Technology), May 2017, 71 pp., 2 tables, 56 figures, 37 numbered references.

This thesis presents the design, modeling, and experiment of a novel pressure sensor using a dual-mode AT-cut quartz crystal resonator with beat frequency analysis based temperature compensation technique. The proposed sensor can measure pressure and temperature simultaneously by a single AT-cut quartz resonator. Apart from AT-cut quartz crystal, a newly developed Langasite (LGS) crystal resonator is also considered in the proposed pressure sensor design, since LGS can operate in a higher temperature environment than AT-cut quartz crystal. The pressure sensor is designed using CAD (computer aided design) software and CAE software - COMSOL Multiphysics. Finite element analysis (FEA) of the pressure sensor is performed to analyze the stress- strain of the sensor's mechanical structure. A 3D printing prototype of the sensor is fabricated and the proposed sensing principle is verified using a force-frequency analysis apparatus. Next to the 3D printing model verification, the pressure sensor with stainless steel housing has been fabricated with inbuilt crystal oscillator circuit. The oscillator circuit is used to excite the piezo crystal resonator at its fundamental vibrational mode and give the frequency as an output signal. Based on the FEA and experimental results, it has been concluded that the maximum pressure that the sensor can measure is 45 (psi). The pressure test results performed on the stainless steel product shows a highly linear relationship between the input (pressure) and the output (frequency).

Copyright 2017

by

Thanh Tuong Pham

ACKNOWLEDGEMENT

First, I would like to express my thanks, sincere gratitude, and appreciation to my Major Professor, Dr. Haifeng Zhang, for his instruction, great support, and motivation to accomplish my thesis. He consistently allowed this paper to be my own work, but steered me in the right the direction whenever he thought I needed it.

Second, I also truly express my thanks to Committee members Dr. Phillip R. Foster and Dr. Shuping Wang for their guidance and invaluable comments on this thesis. Next, I would like to give special thanks Dr. Suresh Kaluvan - a member in Dr. Zhang's lab, other members in the lab, friends, and ETEC department staff for their support during the time I worked on my thesis.

Finally, I would like to thank you my family members for their encouragement, physical and mental support. This thesis could not be accomplished without their contributions.

TABLE OF CONTENTS	Page
ACKNOWLEDGEMENT.....	iii
LIST OF TABLES	vi
LIST OF FIGURES	vii
CHAPTER 1 INTRODUCTION	1
CHAPTER 2 LITERATURE REVIEW	4
2.1 Pressure Measurement and Pressure Sensor	4
2.2 Piezoelectric Material and Piezoelectric Effect.....	9
2.2.1 Piezoelectric Material	9
2.2.2 Piezoelectric Effect.....	11
2.3 AT-Cut Quartz and Langasite Piezoelectric Material	12
2.3.1 AT-Cut Quartz Piezoelectric Material	12
2.3.2 Langasite Piezoelectric Material	13
2.4 Bulk Acoustic Wave (BAW), Surface Acoustic Wave (SAW), and Modes of Vibration ..	14
2.5 Force-Frequency Effect on Crystal Resonator.....	16
2.6 Application of Quartz, Langasite Crystal on Pressure Sensor	19
2.7 Temperature and Resonance Frequency Relation on Crystal Resonator	19
2.8 Dual-Mode and Temperature Compensation.....	21
CHAPTER 3 EXPERIMENT METHODOLOGY	22
3.1 Experiment on Force-Frequency Effect of Crystal Resonator	22

3.1.1 Experiment Procedure	22
3.1.2 Experiment Results	25
3.2 Pressure Sensor Housing Design	27
3.2.1 Operation Principle of the Presssure Sensor	27
3.2.2 Preliminary Design by CAD (Computer Aided Design) Software	28
3.2.3 Finite Element Analysis (FEA) of the Pressure Sensor	31
3.3 3D Printing Prototype.....	38
3.4 Experiment on 3D Printing Prototype.....	38
3.5 Design and Fabrication of Pressure Sensor with Stainless Steel Housing	40
3.6 Experiment on Pressure Sensor with Stainless Steel Housing.....	43
3.7 Crystal Oscillator Circuit Design	47
3.8 Beat Frequency Experiment.....	48
CHAPTER 4 CONCLUSION AND FUTURE RESEARCH.....	54
APPENDIX A DESIGN DRAWINGS OF PRESSURE SENSOR	55
APPENDIX B DESIGN DRAWINGS OF ALL-LANGASITE STRUCTURE.....	64
REFERENCES	67

LIST OF TABLES

Page

Table 1: Maximum Force Applied on Crystal	37
Table 2: Force-Frequency Relation	40

LIST OF FIGURES

Page

Figure 1: Pressure sensor using diametric force application (Hewlett Packard)..... 6

Figure 2: Structures where external hydrostatic pressure applies planar stress patterns in a TSMR disc via a cylindrical shell 7

Figure 3: Pressure sensor using uniaxial stress (Schlumberger)..... 7

Figure 4: Components of the all-langasite sensor structure 8

Figure 5: Unit cell of quartz [16] 10

Figure 6: Direct piezoelectric effect [16] 11

Figure 7: Inverse piezoelectric effect at applied electric field [16] 11

Figure 8: Typical cuts of quartz crystal [18] 13

Figure 9: Modes of vibration of quartz resonator [21]..... 15

Figure 10: Isometric view of an AT-cut quartz crystal resonator 16

Figure 11: Illustration of force application and azimuth angle ψ [29] 17

Figure 12: Force sensitivity coefficients in resonators of different materials and cuts [31]..... 18

Figure 13: Block diagram of the temperature compensation 21

Figure 14: 3D isometric view (a) and front view (b) of the force loading device 22

Figure 15 Pictorial representation of the force loading device 23

Figure 16: Photo of experiment setup..... 24

Figure 17: Definition of azimuth angles ψ for the experiment 25

Figure 18: Force-frequency relation graph at different azimuth angles ψ obtained from LabVIEW 26

Figure 19: The curve K_f of a quartz resonator from the experiment vs. peer’s curve K_f 27

Figure 20: Mounting methods for TSMR using either a two-point mount or a three or four-point mount [21]	28
Figure 21: Dimensions and section view of the pressure sensor	29
Figure 22: Detailed view and side view B of the pressure sensor	29
Figure 23: Section isometric view (a) and exploded view (b) of the pressure sensor.....	30
Figure 24: Subdomains (a, b, c, d) of the analyzed assembly model.....	31
Figure 25: Boundaries (a, b, c, d) of the analyzed assembly model	32
Figure 26: Mesh analysis of the analyzed assembly model.....	33
Figure 27: Stress vs. diametric dimension of the crystal resonator	34
Figure 28: FEA result of stress on a diametric section of the assembly model	35
Figure 29: FEA result of displacement on the assembly model.....	35
Figure 30: FEA result of displacement on a diametric section of the assembly model	36
Figure 31: Linear relationship between the inlet pressure and force applied on the crystal	37
Figure 32: Prototype of the pressure sensor fabricated by a 3D printer	38
Figure 33: (a) Mounting and electrical connection of the crystal, and (b) Fundamental resonance frequency graph of the crystal when the applied force is 0 N	39
Figure 34: (a) Force applied on the box, (b) Force-frequency graph.....	40
Figure 35: Section view of the assembly of the designed pressure sensor.....	41
Figure 36: Detail views of the assembly of the designed pressure sensor.....	41
Figure 37: Bill of material of pressure sensor assembly	41
Figure 38: Mounted crystal on one end cap (holder).....	42
Figure 39: Stainless steel pressure sensor final assembly	42

Figure 40: Final assembly of the pressure sensor with stainless steel housing	43
Figure 41: Diaphragm of the resonance frequency measurement	43
Figure 42: Resonance frequency measurement on mounted crystal	44
Figure 43: Schematic diaphragm of the pressure measurement experiment setup	44
Figure 44: Pictorial diaphragm of the pressure measurement experiment setup.....	45
Figure 45: Pressure measurement experiment and graph result.....	46
Figure 46: Fabricated crystal oscillator circuit.....	46
Figure 47: Pressure measurement result of the designed pressure sensor.....	47
Figure 48: Designed crystal oscillator circuit	48
Figure 49: Fabricated crystal oscillator circuit	48
Figure 50: Diagram of the experiment setup on temperature vs. frequency	49
Figure 51: Photos of the experiment set up for beat frequency vs. temperature.....	50
Figure 52: Crystal resonator mounting and connection in the ceramic box.....	50
Figure 53: 3*fundamental frequency and 3rd overtone frequency vs. temperature in quartz...	51
Figure 54: 3*fundamental frequency and 3rd overtone frequency vs. temperature in LGS.....	52
Figure 55: Beat frequency vs. temperature of quartz	52
Figure 56: Beat frequency vs. temperature of LGS.....	53

CHAPTER 1

INTRODUCTION

Pressure measurement based on piezoelectric crystal resonators has advantages over the commercially available methods like capacitive, electromagnetic, optical, potentiometric, and piezo resistive strain gauge. Since the output of piezoelectric based sensors are digital in format, it has the advantages like very high resolution, high accuracy, and the long-term stability [1]. Quartz is one of the piezoelectric materials commonly used in digital pressure sensors. This material is elastic in nature, providing high stability, high repeatability and elasticity, repeatable mechanical behavior for large cycle of operation, and is free of hysteresis. Quartz crystal resonator (QCR) is commonly used in industry as it has a high Q, which means that very high vibration can be driven with a very low electric power [2]. Furthermore, since the elastic stiffness constant of the QCR is very large, the deformation of this crystal resonator is very small when applied with moderate external force. In pressure sensing aspect, this ensures the linearity of the diaphragm deformation and therefore enhances the linearity of the sensor. Also, the sensitivity of the sensor is closely similar to that of bare QCR because of the small deformation and the thin thickness of the diaphragm. Because of the advantages of quartz and QCR in pressure sensing as stated above, pressure sensors using quartz crystal resonators have been developed and produced. Those pressure sensors have low noise capabilities which can result in very high resolution, and the long-term stability of resonator can ensure the high accuracy output.

Commercial manufacturers such as Hewlett-Packard, Quartztronics, Halliburton, Schlumberger, and Quartzdyne are having different range of pressure sensor products, which

are designed using thickness-shear mode quartz piezo crystals. Currently, most of the pressure sensors use all-quartz structure, which is constructed entirely using a single piece of quartz piezo crystal [3]. For example, the structure of the Quartzdyne's sensor is a thick wall hollow cylinder with closed ends. The thickness-shear mode disc resonator divides the central part of the hollow cylinder. Fluid pressure on the exterior hydrostatically compresses the quartz cylinder, producing internal compressive stress in the resonator. Quartzdyne is the one of the main manufacturer supplying the thickness-shear quartz sensors. The company has developed the pressure sensor by decreasing its size and improving its precision up to 0.02% of full-scale accuracy while being able to measure pressures up to 30,000 psi at 200°C [4].

Despite the good performance, the cost of commercial pressure sensors is very high, their structures are complicated and the temperature affection on pressure measurement has not been minimized completely. Those pressure sensors use three separated crystal resonators to perform temperature compensation: One crystal responses to exposed pressure, the second crystal is sensitive to temperature and the third one as a reference crystal has minimal sensitivity to pressure and temperature [1]. Although this method can yield the temperature compensation through microprocessor, the accuracy of the pressure measurement using this method is affected by thermal lag which occurs when distance between the crystals exists. Meanwhile, dual-mode excitation method can provide superior temperature compensation since the distance between crystals is eliminated. Instead, in dual-mode excitation, two modes occupy the same volume of quartz, and therefore minimize thermal lag problem. Also, the self-sensing of crystal resonator or dual-mode excitation on the crystal can eliminate the temperature control. This can simplify the structure of the sensor. Apart from quartz, Langasite

(LGS) is a new promising piezoelectric material that combines the advantageous properties of quartz with its good performance at high temperatures. LGS will not undergo any phase transitions up to its melting temperature of 1473°C [5]. Hence, the application of Langasite in measuring pressure at high temperature is necessary.

For the reasons mentioned above, this thesis focuses on the design, modeling, and experiment of a novel pressure sensor using a dual-mode AT-cut quartz crystal resonator with beat frequency analysis based temperature compensation technique. A novel mounting structure of the crystal resonator is proposed and the application of LGS circular crystal resonator is also considered in the design. The newly designed pressure sensor has advantages in low cost, high accuracy, and simplified structure. In the proposed pressure sensor, the force sensing element is a commonly used circular AT-cut quartz crystal resonator, which is mounted in the two caps and excited by two modes of vibration simultaneously: fundamental mode and third overtone mode. The pressurized air from the inlet is totally separated from the quartz crystal by a diaphragm. An oscillator circuit which excites the crystal resonator at fundamental vibration mode is fabricated. To verify the performance of the fabricated pressure sensor, a pressure measurement is performed on the pressure sensor at fundamental mode of vibration and the temperature-frequency relation experiment on both quartz and LGS crystal resonators is performed.

CHAPTER 2

LITERATURE REVIEW

2.1 Pressure Measurement and Pressure Sensor

Pressure measurement is critical and common in fields such as metrology, aerospace, hydrology, process control, meteorology, energy exploration, and oceanography. A pressure transducer is a device that measures pressure and converts it to other means of measurement elements such as displacement, inductance, resistance, optical signal, frequency, and capacitance. In general, analog and digital are two basic categories of pressure sensors.

In analog pressure sensors, the input signal is the pressure of the environment. The output is the analog signal or continuous signal. Typical analog pressure sensors are piezoresistive strain gauges (either bonded or formed) using piezoresistive effect to detect strain due to applied pressure, with resistance increasing as pressure deforms the material. Capacitive pressure sensors use a diaphragm and a pressure cavity to create a variable capacitor to detect strain caused by applied pressure, with capacitance decreasing as pressure deforms the diaphragm. Electromagnetic pressure sensors measure the displacement of a diaphragm by means of changes in inductance. Optical pressure sensors employ a technique using the physical change of an optical fiber to detect strain caused by applied pressure. Thermal pressure sensors use changes in thermal conductivity of a gas caused by density changes to measure pressure. In dynamic pressure sensors, the direct piezoelectric effect is utilized. That means, when a force is exerted upon a piezoelectric element, a voltage is generated.

In digital pressure sensor, the signal of the output is digital (resonant) since it is a frequency signal. Although there are many resonance based sensors, the most commonly used especially in oil field is digital quartz crystal sensor. There are two basic types of digital quartz sensors: thickness-shear mode resonator (TSMR) found in Hewlett-Packard design and the vibrating beam made popular by Paroscientific [6]. The thickness-shear mode digital quartz sensor is a hydrostatic pressure sensor, since the sensing element is totally surrounded by a pressure media. The vibrating beam device is a force sensor when the pressure must be converted to a force by means such as Bourdon tube, and a structure combining bellows, hinges, and levers. Each type has its strengths and weaknesses. The thickness-shear mode quartz sensor is based upon the well-known force-frequency effect of precision quartz resonators. The force-frequency effect occurs when a force is exerted upon the circumference of a quartz resonator and its resonant frequency will shift in proportion to the applied force.

Quartzdyne is a main supplier of digital (resonant) pressure sensor using an all-quartz structure. A typical model of Quartzdyne's pressure sensor is TMC16K-B, which has a pressure range of 16,000 psi and a temperature range of 177⁰C [6]. The transient performance of Quartzdyne's pressure transducers (pressure sensors) has been developed, but there is still more work to be done on the transient performance improvement for certain products [7].

In all-quartz structure pressure sensor, EerNisse [8] categorized the pressure sensor into four groups: (1) Pressure sensor using diametric force application as in Figure 1, (2) pressure sensor using uniform stress as in Figure 2, (3) pressure sensor using uniform stress and a diametric force component, and (4) pressure sensor using uniaxial stress as in Figure 3.

Karrer and Ward [8] also constructed an all-quartz structure to measure pressure. In their research, a quartz diaphragm squeezes on a diameter of an AT-cut quartz resonator as seen in Figure 1. The direction of the force axis is the crystallographic axis of crystal, which has the largest force-frequency effect coefficient. The all-quartz structure helps avoid differences in thermal expansion. Force is applied from the diaphragm and base to the disc edges by devitrifying glass joints [6]. This structure can be commonly found in Hewlett Packard (HP) devices.

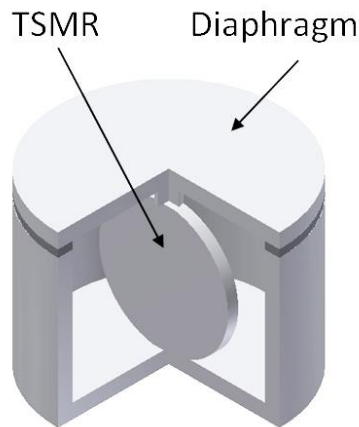


Figure 1: Pressure sensor using diametric force application (Hewlett Packard)

Figure 2a shows an all-quartz structure including a resonator disc which is squeezed uniformly around the perimeter. When the structure is put in a pressure environment, a uniform radial stress two to three times the applied pressure occurs in the resonator. The structure has been improved, and the one used by Quartzdyne has smaller size and lower cost than previous designs [8]. Use of non-uniform stress in the resonator would provide a new degree of freedom to optimize the sensor performance. As in Figure 2b, flatten surface is added to break the symmetry of the shell adding more degree of freedom for the pressure sensor.

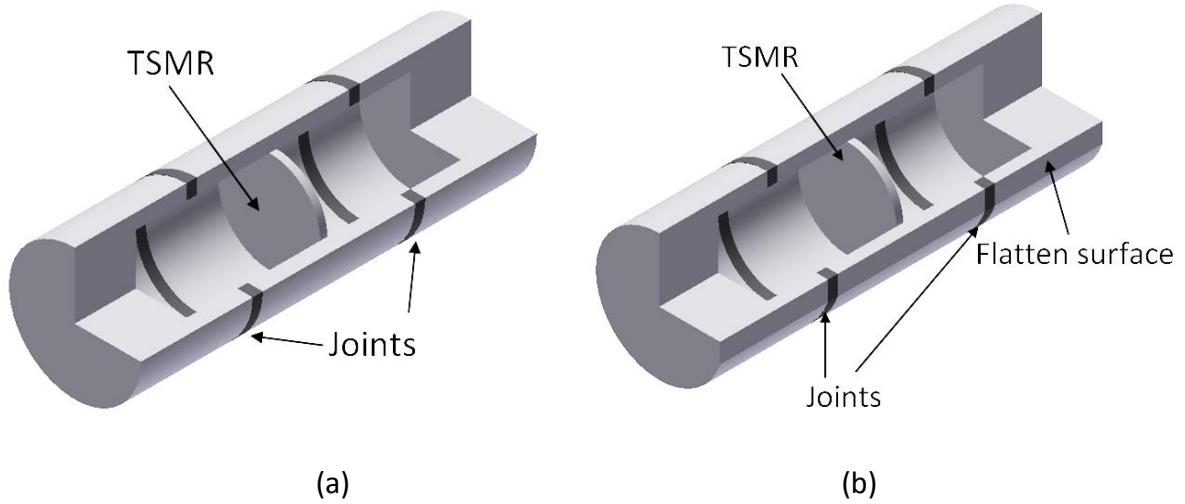


Figure 2: Structures where external hydrostatic pressure applies planar stress patterns in a TSMR disc via a cylindrical shell

(a) Uniform radial stress (Hewlett Packard and Quartzdyne)

(b) Superposition of diametric force effect and uniform radial stress from the presence of deep flats (Halliburton)

Figure 3 shows a structure where external pressure of the structure applies a uniaxial stress in a TSMR plate through a cylindrical shell [8].

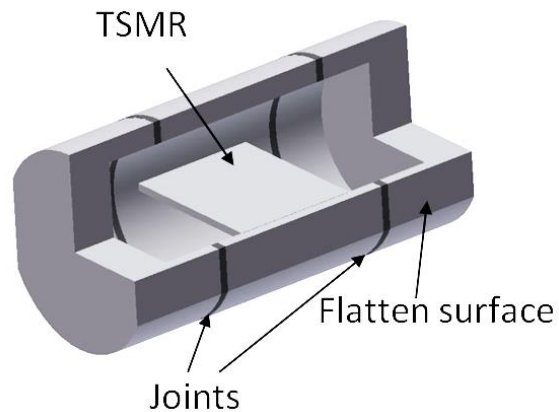
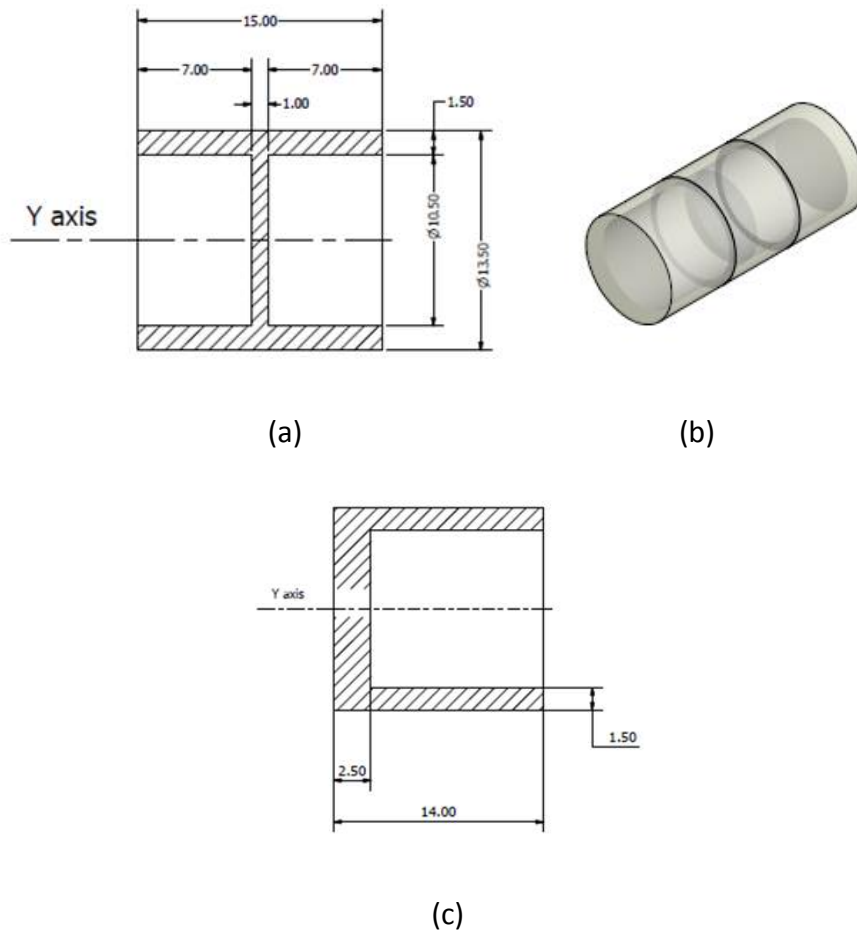


Figure 3: Pressure sensor using uniaxial stress (Schlumberger)

Figure 4a, b, and c introduce views of a designed all-langasite structure of pressure sensor for future experiment on its performance at high temperatures. The structure has three parts: two end caps and the middle section that integrates crystal resonator disc. The two end caps are bonded with the middle section hermetically by a devitrifying glass joint. The whole structure is made of langasite in order to minimize the thermal expansion, which affects the accuracy of the pressure measurement. Detailed design drawings of these parts can be found in Appendix B.



(a) Section view of crystal resonator (b) Isometric view of the structure
(c) Section view of the crystal cap

Figure 4: Components of the all-langasite sensor structure

Karrer and Leach [9] calculated and designed a pressure transducer using a single quartz crystal structure. A cylindrical quartz tube integrated with the circular resonator acts as a diaphragm. Temperature control system and the complicated structure can cause high cost on the manufacture of the pressure sensor [10]. Besson [11] presented a design of dual-mode thickness shear quartz pressure sensor to retrieve the applied pressure and the in-situ temperature of the sensor from the same resonator. This resonator employs doubly rotated cuts of quartz. Asakura [12, 13] developed a compact force pressure sensor using an AT-cut quartz crystal resonator and a new retention mechanism of the resonator. The maximum load is 45 N and the measurement range is 10^4 . The new retention mechanism of the AT-cut quartz crystal resonator was improved by Keisuke group [14]. In Keisuke's new design, the hysteresis caused by friction in the previous design [12, 13] was eliminated by using a new retention mechanism. The improvement on sensor resolution and miniaturization has also been achieved.

Besides bulk acoustic wave (AT-cut quartz crystal resonator) based pressure sensor, Lucia [15] proposed a new approach for high pressure measurement using surface acoustic wave (SAW). According to Lucia, the sensor can be cost effective and have higher sensitivity as compared to commercial sensors.

2.2 Piezoelectric Material and Piezoelectric Effect

2.2.1 Piezoelectric Material

Piezoelectric materials can be natural or man-made. The natural piezoelectric materials are crystal materials such as quartz (SiO_2), Rochelle salt, Topaz, and Tourmaline-group minerals and some organic substances such as silk, wood, enamel, dentin, bone, hair, and rubber. Figure 5 shows the unit cell of quartz, which has a specific atomic structure of the lattice. The lattice is

a tetrahedron built of oxygen atoms around a silicon atom. Each oxygen atom is located at the same distance to the silicon atom, and the distances between the oxygen atoms are all the same. The change in the position of the atoms due to applied stress leads to the formation of net dipole moments that causes polarization and an electric field, respectively. Man-made piezoelectric materials include Barium Titanate, and Lead Zirconate Titanate.

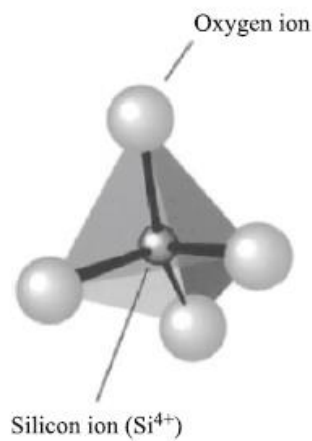


Figure 5: Unit cell of quartz [16]

Piezoelectricity as a research field in crystallographic physics was initiated by the brothers Jacques Curie (1856–1941) and Pierre Curie (1859–1906) with their studies. They discovered an abnormal characteristic of certain crystalline minerals including tourmaline, quartz, topaz, cane sugar, and Rochelle salt. They found that when the tension or compression force is applied on the crystal, voltages are generated of opposite polarity and proportional to the applied load. This is called the direct piezoelectric effect.

2.2.2 Piezoelectric Effect

The direct piezoelectric effect is shown schematically in Figure 6a and b. The word piezoelectricity comes from Greek word piezo (pressure) and refers to electricity resulting from pressure. In the year following the discovery of the direct effect of crystal resonator, Lippman predicted the existence of the inverse effect basing on fundamental thermodynamic principles. Before the end of 1881, the Curie brothers experimentally verified the existence of the inverse effect. They proved that if a piezoelectric material was exposed to an electric field, it would lengthen or shorten in accordance with the polarity of the field, and in proportion to its strength. This inverse effect is illustrated in Figure 7a and b [16].

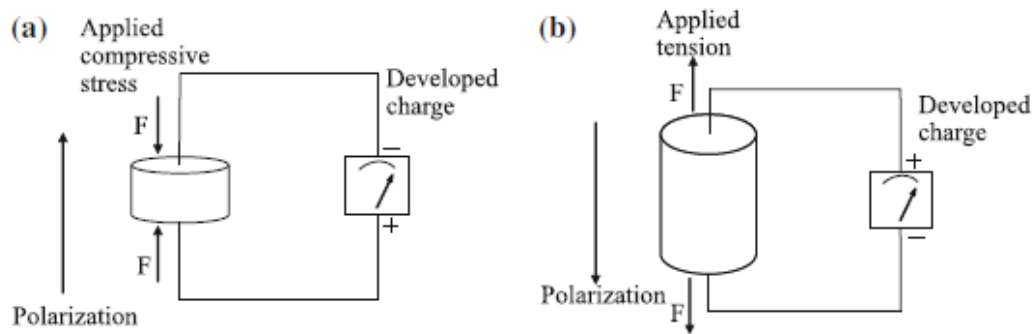


Figure 6: Direct piezoelectric effect [16]

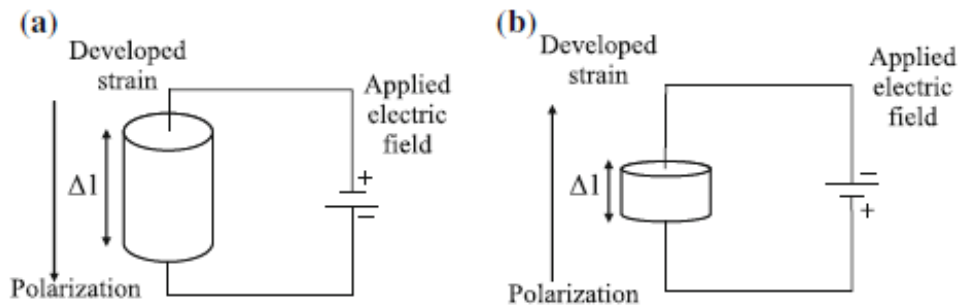


Figure 7: Inverse piezoelectric effect at applied electric field [16]

The piezoelectric effect is very useful in many applications that involve the production and detection of sound, structure health monitoring, electronic frequency generation, microbalances, and sensor technology. Some piezoelectric materials contain toxic substances such as lead (Pb), which is harmful to humans and the environment. Therefore, the demand for more environmentally safe options resulted in the development of new lead-free piezoelectric materials.

2.3 AT-Cut Quartz and Langasite Piezoelectric Material

2.3.1 AT-Cut Quartz Piezoelectric Material

Quartz is the crystalline form of silicon dioxide, SiO_2 , and one of the most common naturally occurring crystalline minerals. It is a hard, brittle, transparent material with a density of $2,649 \text{ kg.m}^{-3}$, and a melting point of $1,750^\circ\text{C}$ [17]. When quartz is heated to 573°C , its crystalline form changes. Most of the physical properties of a crystal are anisotropic (direction dependent). Therefore, changes during the growth of the crystal which affect anisotropy result in crystal imperfections. The major axis of quartz growth is called the optic axis. This axis is not anisotropic to light, so light passes readily. The optic axis is labeled the Z axis in an orthogonal X, Y, and Z coordinate system. A quartz crystal having six sides has three separate X axes and three Y axes definable at 120° increments about the Z axis.

A small piece of quartz material is obtained by cutting the crystal at specific angles to the various axes. The choice of axis and angles determines the physical and electrical parameters for the resonator. These more common cuts provide various trade-offs between electrical-mechanical capability and temperature coefficient. Figure 8 shows typical cuts of a quartz crystal.

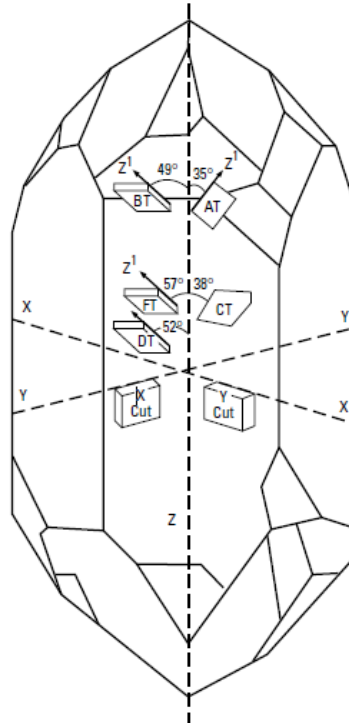


Figure 8: Typical cuts of quartz crystal [18]

The AT-cut quartz thickness shear mode resonator provides a high resonance frequency and exhibits superior temperature stability near room temperature than that of other kinds of vibration modes. Therefore, it is considered to be an applicable material for use in pressure and force sensors. By applying an external force to the quartz crystal resonator, its resonance frequency changes proportionally to the external force. A previous investigation showed that when adding an external force from the direction of 34.8° of X axis of the AT-cut quartz crystal resonator, the stress sensitivity improved mostly.

2.3.2 Langasite Piezoelectric Material

Langasite ($\text{La}_3\text{Ga}_5\text{SiO}_{14}$), Langatate ($\text{La}_3\text{Ga}_5.5\text{Ta}_{0.5}\text{O}_{14}$), and Langanite ($\text{La}_3\text{Ga}_5.5\text{Nb}_{0.5}\text{O}_{14}$) single crystals (LGS, LGT, and LGN, respectively; collectively called LGX) are a group of emerging piezoelectric materials which have been shown to exhibit stable properties

similar to quartz and high electromechanical coupling coefficients similar to lithium niobate. LGS and its isomorphs exhibit quality and electromechanical coupling factors which are, respectively, four and two times greater than those of quartz [19]. One of the most important features of LGX is its phase transition, which occurs under high temperature at its melting temperature of 1,473°C and under high pressure at 10 GPa. These excellent properties of LGS and its isomorphs provide promising applications on sensors and timing in high-temperature and high-pressure environment such as oil and gas industry. Combined with the high Q, the material is promising for yielding lower acceleration sensitivity and lower noise resonators than quartz.

Piezoelectric resonators based on Langasite and its isomorphs have strong piezoelectric coupling, low acoustic loss, zero temperature coefficient of frequency, and reduced nonlinear effects occurring in simple orientations [20]. Therefore, the application of Langasite in pressure sensors to measure pressure and temperature is promising.

2.4 Bulk Acoustic Wave (BAW), Surface Acoustic Wave (SAW), and Modes of Vibration

Bulk acoustic wave (BAW) is elastic waves propagating in solids or substrate. BAW includes longitudinal and transverse waves. The most commonly used BAW devices are the thickness shear mode resonator (TSMR) and the shear-horizontal acoustic plate mode (SH-APM) sensor.

If the wave propagates on the surface of the substrate, it is known as a surface acoustic wave (SAW). The most widely used surface acoustic wave devices are the SAW sensor and the shear-horizontal surface acoustic wave (SH-SAW) sensor, also known as the surface transverse wave (STW) sensor.

The modes of vibration depend on how the crystal was cut. For example, an X-cut crystal exhibits an extensional vibration mode whereas the AT-cut crystal, which is cut at 35 degrees off the Y-axis, vibrates in the thickness shear mode. An illustration of the various vibration modes of quartz resonator is given in Figure 9.

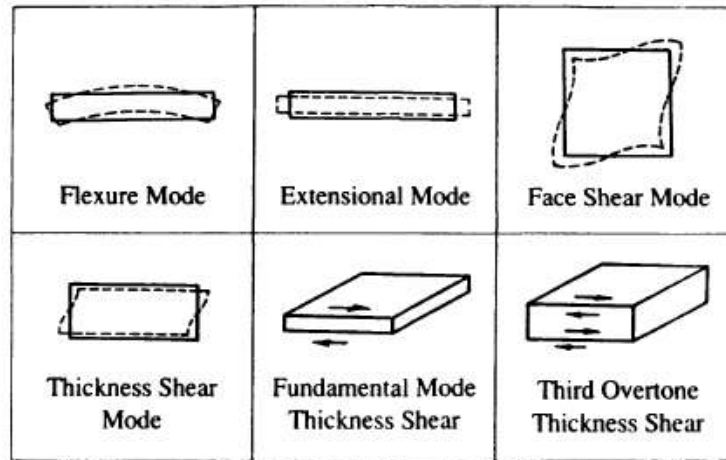


Figure 9: Modes of vibration of quartz resonator [21]

The thickness-shear mode resonator (TSMR) widely referred to as a quartz crystal is the best-known, oldest, and simplest acoustic wave device. The TSMR typically consists of a thin disk of AT-cut quartz with parallel circular electrodes patterned on both sides. The application of a voltage between these electrodes results in a shear deformation of the crystal. This device is known as a resonator because the crystal resonates as electromechanical standing waves are created. Figure 10 shows an isometric view of the AT-cut quartz crystal resonator. In, TSMR, the displacement is maximized at the crystal faces, making the device sensitive to surface interactions. TSMR offers stability, low power, frequency output, and high Q factor due to energy trapping. These properties are critical for frequency control applications and also beneficial in sensor technology.

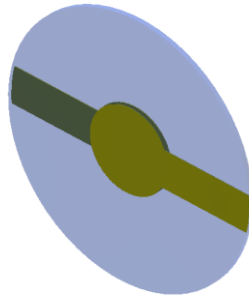


Figure 10: Isometric view of an AT-cut quartz crystal resonator

The vibration frequency is determined by the size and shape of the resonator. For instance, a 10 MHz fifth overtone unit has 1.2 centimeters in diameter and about 1.06 mm in thickness. The primary frequency determining factor for the AT cut and BT cut is the thickness since they vibrate in the thickness shear mode.

2.5 Force-Frequency Effect on Crystal Resonator

The force-frequency effect is the correlation between the force applied on the crystal resonator and the relative response resonant frequency of the resonator to the applied force. The measurement of this effect could provide an important reference for force and pressure sensor design [8], [22]. Experimental research on the force-frequency effect for quartz resonators has been performed for many years. Ratajski [23] measured the force-frequency effect of several singly rotated quartz crystal resonators. Ballato and EerNisse [24], [25] measured the force-frequency effect for doubly rotated quartz resonators. The first measurement of the force-frequency effect in Langasite resonators was published by Boy, et al. in 2001 and the force-frequency effect of Langanite (LGN) resonators was subsequently measured by Kim and Ballato [26]. The first examination of the force–frequency effect in Langasite was published by Boy et al. in 2001 [27].

The prime parameters affecting the force sensitivity of circular crystal resonator are the orientation angle, direction of force, crystal geometry, operating frequency, and the design of the crystal holder [28].

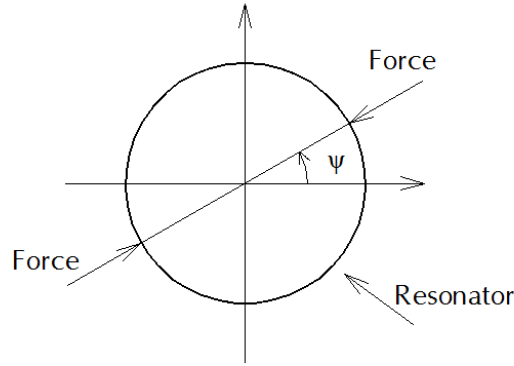


Figure 11: Illustration of force application and azimuth angle ψ [29]

As illustrated in Figure 11, azimuth angle ψ is the angle between the applied force direction and the crystallographic axis of a singly rotated cut crystal.

A more thorough theoretical analysis of the force-frequency effect for doubly rotated Langasite resonators can be found in [20]. The force-frequency effect produced in a circular crystal plate acted upon by diametric in-plane force at the angle ψ is characterized by means of a force-frequency coefficient K_f (m.s/N), which is defined by:

$$K_f = \frac{\Delta f}{f} \cdot \frac{(\text{Diameter})(\text{Thickness})}{(\text{Force})(\text{Acoustic velocity}/2)} \quad (1)$$

Where $\frac{\Delta f}{f}$ is the normalized frequency change due to the applied force [11].

The sensitivity of the resonance frequency can be reduced by selecting correct support orientations. The value of K_f m.s/N can be positive, negative, or zero.

When the force-frequency relation is identified at a certain azimuth angle, this relation is linearized, and the slope of the line can be determined. The coefficient K_f can also be calculated by the following formula:

$$K_f = \frac{df}{dF} \cdot \frac{D}{f_0^2} \quad (2)$$

Where df/dF is the slope of the line (Hz/Newton), D is the diameter of the resonator (m), and f_0 is the frequency (Hz) without force (0 Newton) [30].

Zhang [20] has analyzed the force-frequency relation in Langasite theoretically and numerically and found the developed theory has good agreement with previous experimental results.

Kosinski [31] measured the K_f of Langasite (LGS) and compared it with that of quartz. The K_f of LGS is smaller than that of quartz as shown in Figure 12.

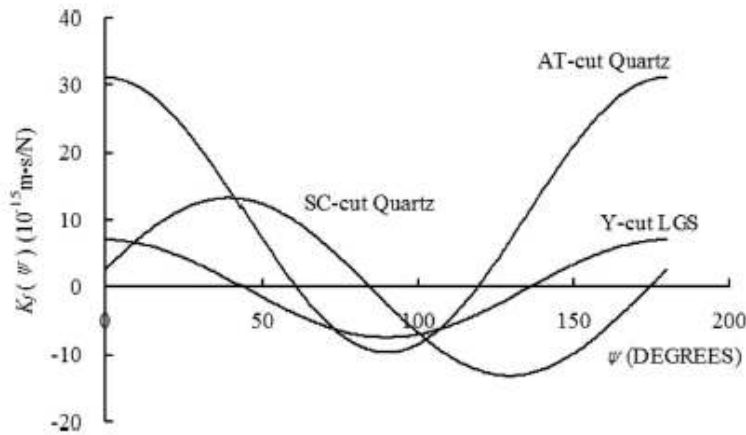


Figure 12: Force sensitivity coefficients in resonators of different materials and cuts [31]

2.6 Application of Quartz, Langasite Crystal on Pressure Sensor

As aforementioned, quartz resonators have been used in many pressure sensor applications and have good performance. Langasite, a new piezoelectric material, can be used in pressure measurement since it has outstanding temperature behavior with a zero temperature coefficient compared to quartz crystal, good piezoelectric coupling, low acoustic loss, and a high Q factor. Many manufacturers such as Hewlett-Packard, Quartztronics, Halliburton, and Schlumberger have applied quartz for their pressure sensors. Manufacturers have been conducting more researches to produce a sensor with higher performance. Factors that affect the performance of the sensor are aging (short-term, long-term), drive energy, gravity, shock, vibration, electromagnetic, retrace, hysteresis, and crystal holder. The effect of a crystal holder on the force-frequency effect was calculated by Ratajski [29]. Furthermore, Langasite is a piezoelectric material that can work at high temperature. Many researches have been performed on this material to verify its performance on the measurement of pressure at high temperature.

2.7 Temperature and Resonance Frequency Relation on Crystal Resonator

The temperature dependence of the resonance frequency of the bulk acoustic wave crystal resonators is a function of material constants, thermal expansion coefficients, coupling between the vibration modes and the nature and the thickness of the electrode. In Y-cut Langasite, the relationship between temperature and frequency is parabolic on fundamental, third, and fifth overtone frequencies [32]. In the AT-cut quartz crystal resonator, both the fundamental and the third overtone mode frequencies are functions of the temperature and force. Because the temperature affects the frequency of the excited crystals as mentioned, it

will reduce the accuracy of the pressure measurement. As a result, the temperature compensation in pressure measurement of AT-cut quartz and LGS crystal based pressure sensor is indispensable.

The beat frequency is defined as the formula:

$$f_b = 3f_1 - f_3 \quad (3)$$

After derivation, the relationship between the normalized beat frequency and the temperature is as follows:

$$\frac{\Delta f_b(T)}{f_b(T)} = \frac{3T_{f,1}^{(1)} - \lambda T_{f,3}^{(1)}}{3 - \lambda} \Delta T \quad (4)$$

Where $T_{f,1}^{(1)}$ is the function of T_0 and T .

$\Delta T = T_0 - T$, T_0 is the reference temperature, and T is the arbitrary temperature.

$\lambda \approx 3$ for AT-cut quartz resonators.

From formula (4), it can be seen that the normalized beat frequency is a linear function of temperature and does not relate to force. Therefore, the beat frequency can be used to measure temperature [33].

2.8 Dual-Mode and Temperature Compensation

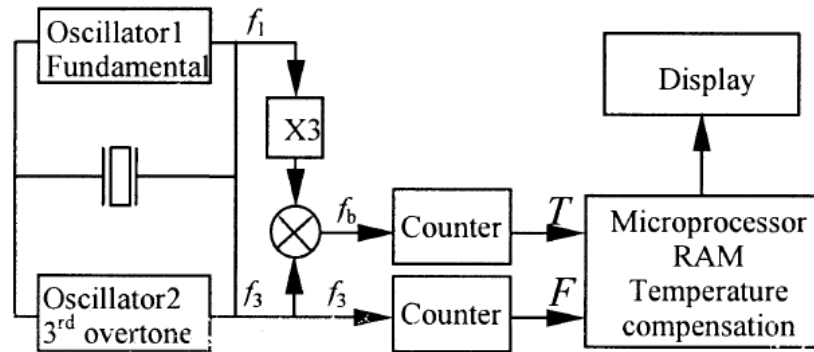


Figure 13: Block diagram of the temperature compensation of a QCR based pressure sensor [34]

The crystal resonator is excited at fundamental mode and third overtone mode simultaneously by oscillator 1 and oscillator 2. The frequency shift of the third overtone mode is used to measure the force, and the beat frequency is used to measure the temperature. A microprocessor functions as a temperature identifier according to the beat frequency, and then it compensates temperature in force or pressure measurement using calibration equation [8], [25], [35].

CHAPTER 3

EXPERIMENT METHODOLOGY

3.1 Experiment on Force-Frequency Effect of Crystal Resonator

3.1.1 Experiment Procedure

The graph of force-frequency coefficient K_f illustrates the positions of azimuth angles where the K_f reaches the greatest value or $K_f = 0$. Based on this graph, the positions of the applied force on the circumference of the crystal resonator, which maximize the force-frequency effect, are identified. The force/pressure sensor's sensitivity increases when the force-frequency effect increases. As a result, in the designed pressure, the position where the mounting and force applied positions of the crystal resonator is determined to increase the performance of the pressure sensor. On the other hand, the performance in frequency control application can be increased by choosing the mounting or holding positions of the crystal where K_f has smallest value. In the research, a force loading device which is used for the measurement of force-frequency effect was designed and manufactured as shown in Figure 14.

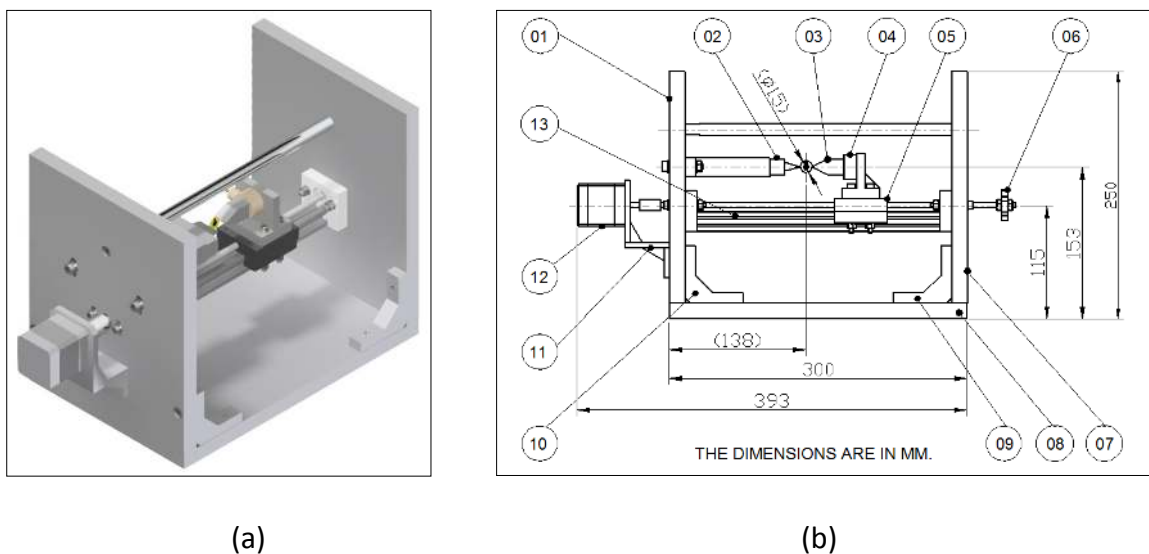


Figure 14: 3D isometric view (a) and front view (b) of the force loading device

Figure 15 shows a pictorial presentation of the experiment using the force loading device. The graph of the force-frequency relationship can be seen from the LabVIEW interface on the computer screen.

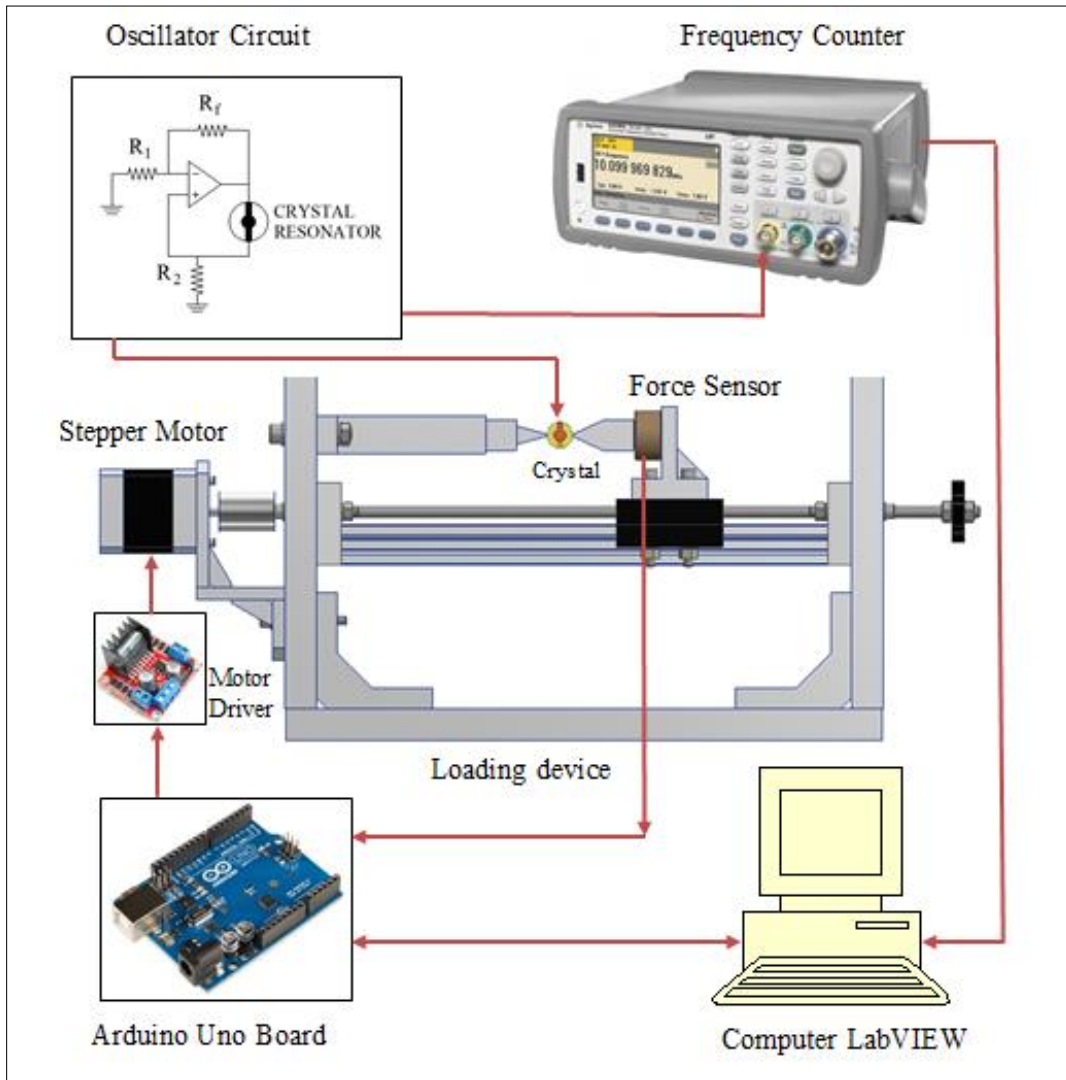


Figure 15 Pictorial representation of the force loading device

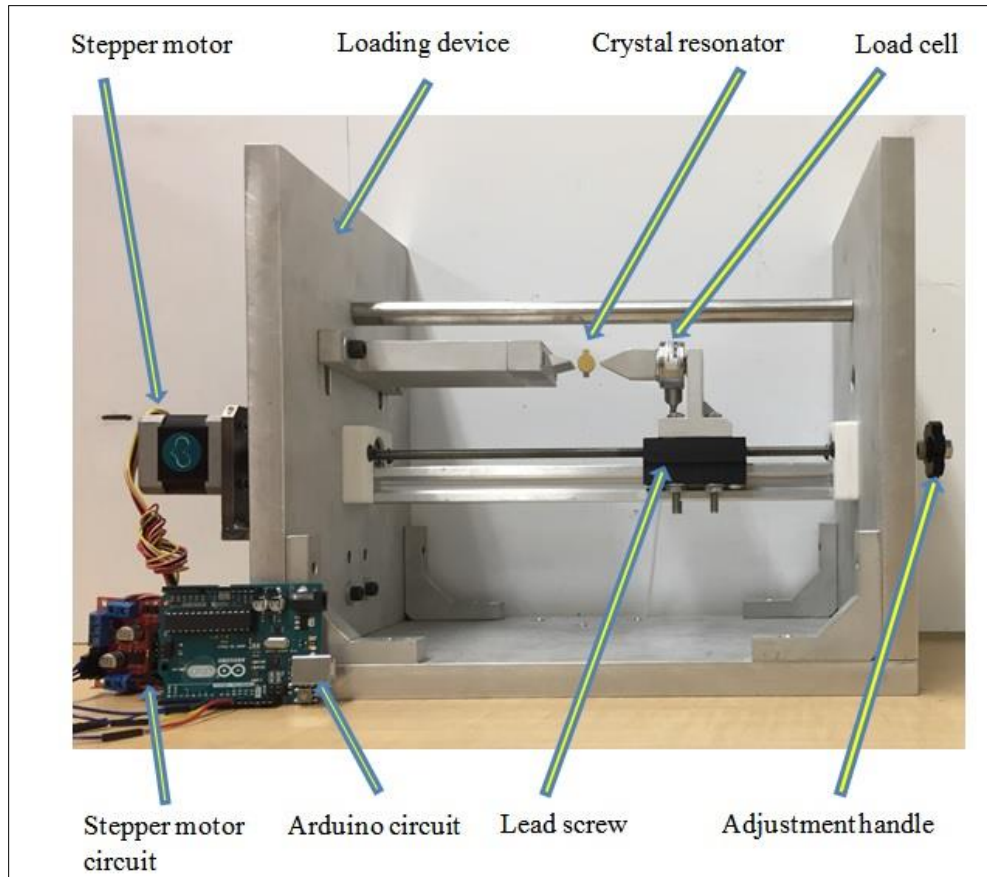


Figure 16: Photo of experiment setup

Figure 16 illustrates a connection setup of the experiment. Firstly, we connect two electrodes of the crystal resonator to the crystal oscillator circuit. The input of the crystal oscillator circuit is DC current. This circuit excites the crystal resonator and the AC frequency output of the circuit is connected to the frequency counter.

In manual mode, the handle of the lead screw (06 in Figure 2b) is rotated to apply force on the crystal. The value of the applied force is shown on the digital indicator. The relative output frequency value is read from the frequency counter. The relationship between the applied force and the output frequency can be plotted from those two values. Based on formula (2), we can calculate the force-frequency coefficient K_f at one azimuth angle. The

crystal resonator can be rotated so that we can calculate K_f at different azimuth angles. Finally the plot of K_f vs. azimuth angle can be drawn.

In automation mode, the crystal resonator is mounted similarly to the manual mode. However, the maximum applied force is specified in the LabVIEW interface (for example 40 N), then press the RUN button. The force applied on the crystal is increased and measured over time automatically. At the same time, the output frequency is measured. The graph of the input force and the output frequency is yielded and shown on the LabVIEW interface. Likewise, the plot of K_f then can be obtained.

3.1.2 Experiment Results

Example experimental results have been obtained for an AT-cut quartz resonator. The diameter and thickness of this quartz resonator is 15 mm and 0.335 mm relatively. Figure 17 shows the typical azimuth angles where the tips of the clamps contact and apply force on the resonator. Because of the physical shape of the measured crystal resonator, the azimuth angles for the experiment are defined at these values: 0° , 10° , 20° , 30° , 40° , 50° , 60° , 70° , 80° , 110° , 120° , 130° , 140° , 150° , 160° , 170° and 180° .

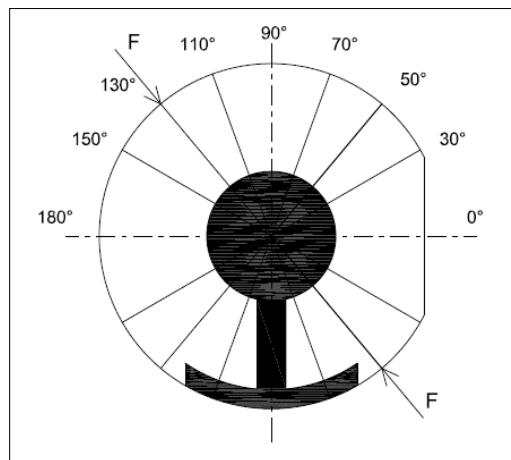


Figure 17: Definition of azimuth angles ψ for the experiment

The graph in Figure 18 shows force-frequency graph obtained from LabVIEW at aforementioned azimuth angles. The linear relation between force and frequency is found from the graph. The force-frequency relation is measured when the force is increased and decreased. The hysteresis error is small when using the designed apparatus. The force sensitivity coefficients K_f are calculated based on formula (2) and plotted in Figure 19. This result shows a good agreement with peers' measurement results in [12], [14], [15].

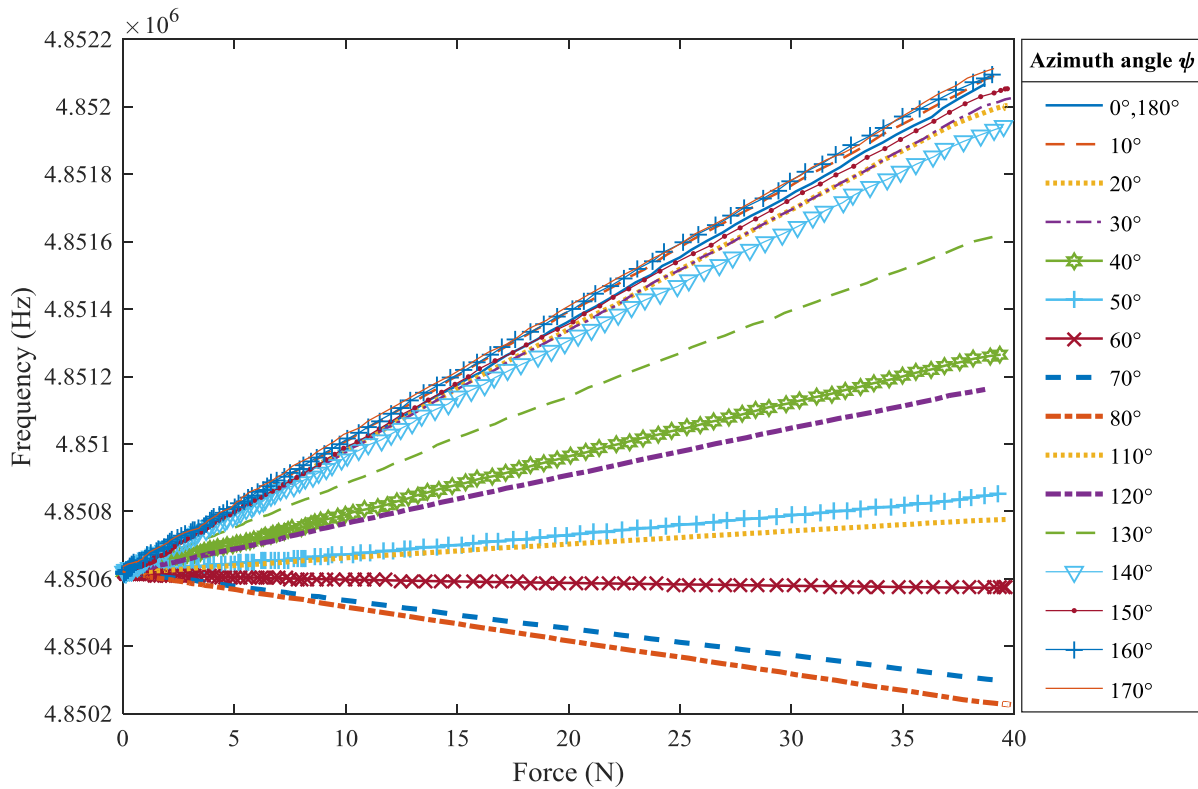


Figure 18: Force-frequency relation graph at different azimuth angles ψ obtained from LabVIEW

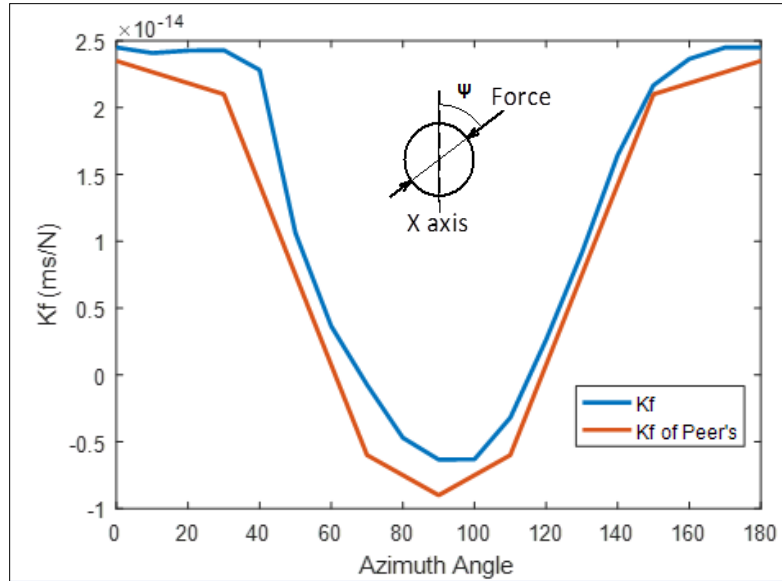


Figure 19: The curve K_f of a quartz resonator from the experiment vs. peer's curve K_f

3.2 Pressure Sensor Housing Design

3.2.1 Operation Principle of the Pressure Sensor

The mounting box is comprised of two circular caps. The AT-cut quartz crystal resonator is placed inside box. When a air pressure at the inlet exists, the diaphragm will deform and apply force on the crystal through the upper cap of the box. This will then create the force-frequency effect on the crystal resonator. Based on the frequency shift relative to the applied force on the crystal, we can measure the relative inlet pressure of the environment. To compensate temperature affection on the accuracy of the pressure measurement, one crystal resonator is excited at fundamental frequency and 3rd overtone mode simultaneously. The diameter of the used AT-cut quartz crystal resonator is 0.591 inch, the thickness is 0.015 inch and the resonance frequency is 5.297 MHz.

3.2.2 Preliminary Design by CAD (Computer Aided Design) Software

The material of the diaphragm can be quartz [36] or stainless steel. The stainless steel 303 is used in the proposed sensor since this material can resist corrosion especially in a corrosive medium such as gas, oil environment, and this material is also durable and has good machinability.

To minimize the mounting and acceleration effects on frequency stability, the location of the mounting points of the crystal resonator where the force-frequency coefficient $K_f = 0$ needed to be identified. Based on the results of the experiment and the graph of K_f [30], we can identify suitable positions to mount the crystal resonator. Figure 20 illustrates typical mounting methods of the crystal resonator.

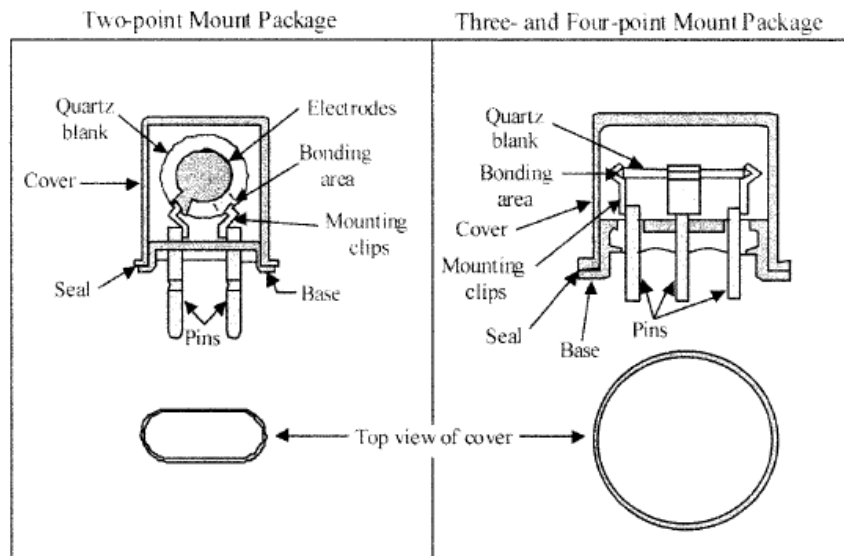


Figure 20: Mounting methods for TSMR using either a two-point mount or a three or four-point mount [21]

Figure 21 shows a section view of the sensor. The part including a diaphragm is assembled with the housing by thread. The opposite side of this housing is the crystal holders (two end caps) that keep the crystal inside. The connecting nut connects the housing of the crystal holders and the housing of the oscillator circuit.

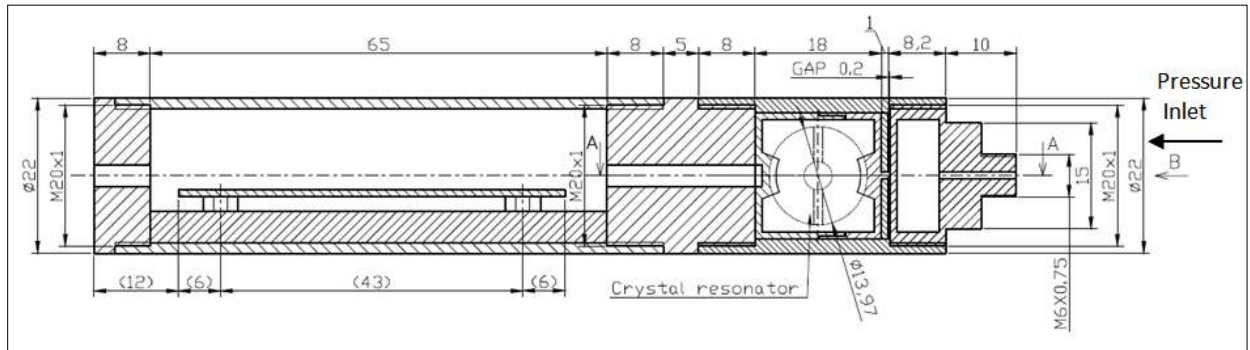


Figure 21: Dimensions and section view of the pressure sensor

Figure 22 shows detailed view of the crystal area and the view of the air pressure inlet. One end cap of the crystal holder has a pin that goes through the middle wall of the housing and contacts the diaphragm. When there is air pressure in the inlet, the diaphragm is bended and it pushes the pin of the crystal holder. Hence, the crystal is compressed by a diametric force, the frequency of the crystal is shifted. Based in this signal, the air pressure of the inlet can be determined. View B in Figure 22 show the hexagon nut which is hollow so that air pressure can go inside and the nut can be rotated to assemble with the housing.

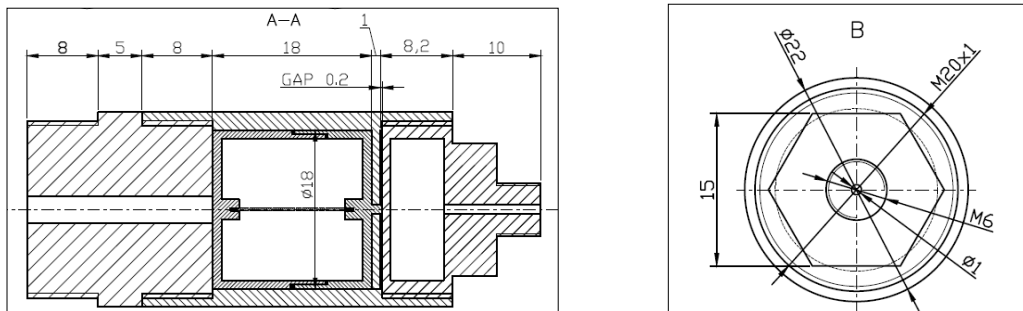
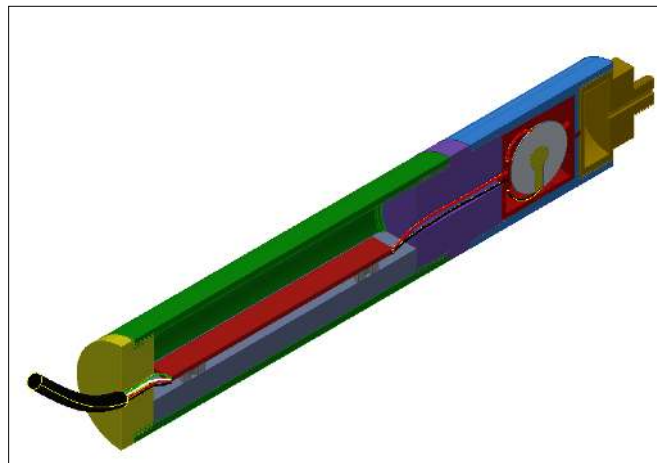
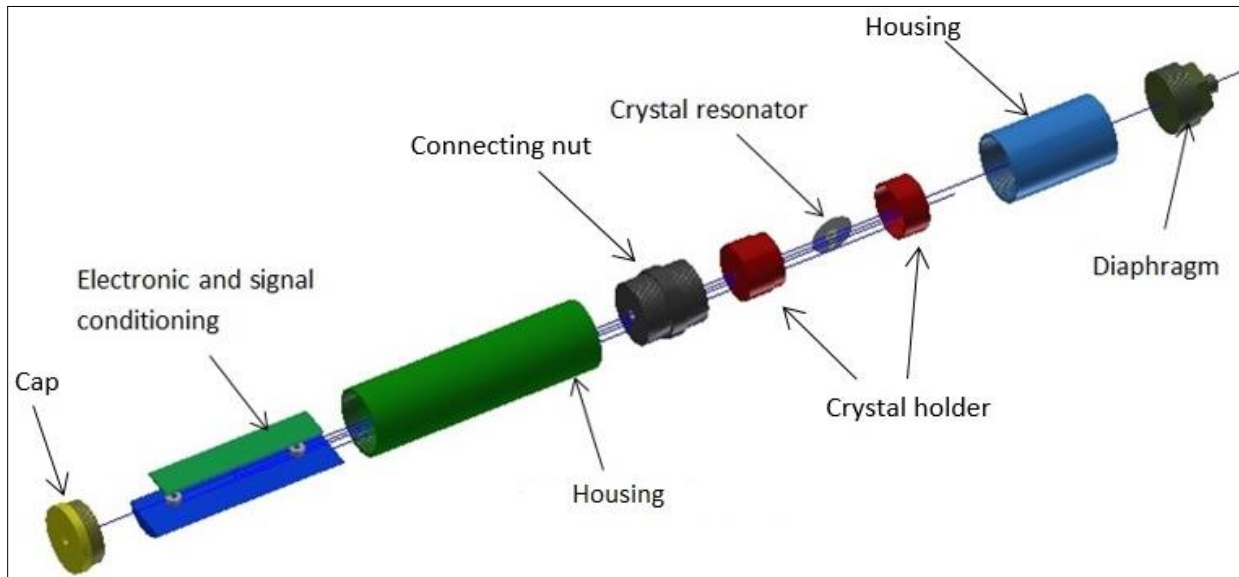


Figure 22: Detailed view and side view B of the pressure sensor

Figure 23a and b are the 3D section view and the exploded view of the assembly. The section view shows all parts of the pressure sensor and electrical connection. The two electrodes of the crystal are connected to the oscillator circuit by electrical wires. The other side of the circuit is linked to power supply and frequency output. The exploded view illustrates named parts arranged along an axis of the pressure sensor.



(a)



(b)

Figure 23: Section isometric view (a) and exploded view (b) of the pressure sensor

3.2.3 Finite Element Analysis (FEA) of the Pressure Sensor

The COMSOL Multiphysics software is used to perform finite element simulation on the designed pressure sensor. The assembly including the diaphragm, two caps and the crystal resonator is analyzed. The 3D model of this assembly is imported to the COMSOL in STEP file format. The details of the finite element analysis of the assembly are described as follows:

First, the model is divided into 4 subdomains as shown in Figure 24. The materials for those subdomains are also selected: The material for highlighted subdomains in Figure 24a, c, and d is stainless steel. In Figure 24b, the material for the highlighted subdomain is quartz, and the material type of this subdomain is anisotropic. Also, the force direction applied on the crystal is parallel with the X axis of the model and the crystal.

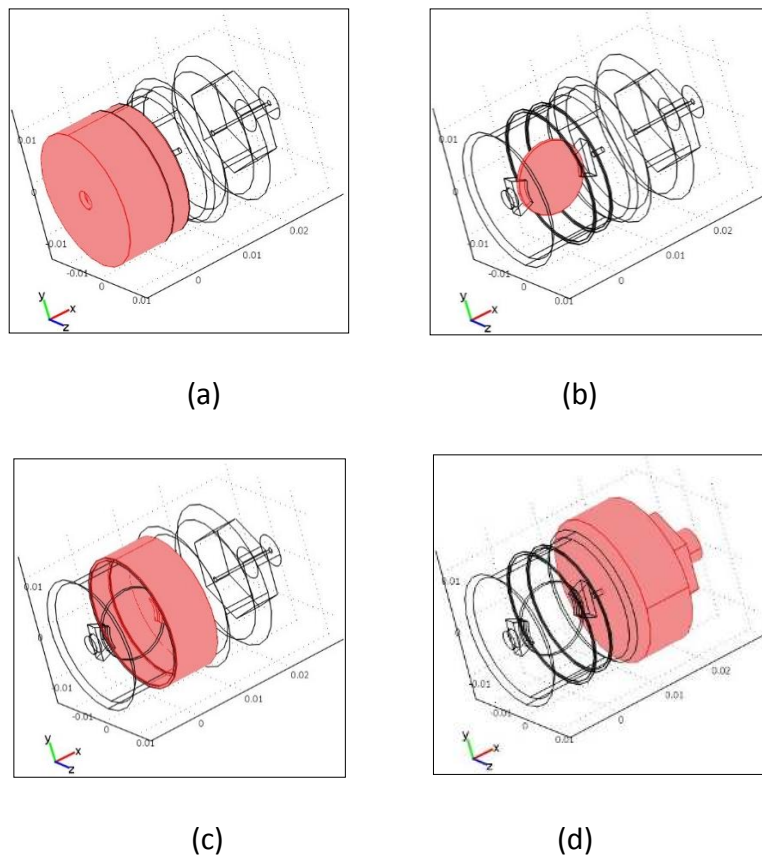


Figure 24: Subdomains (a, b, c, d) of the analyzed assembly model

Next, the boundary conditions are applied for the model. There are total 72 boundaries in the analyzed model as indicated in COMSOL. The highlighted boundaries as shown in Figure 25a, b, c are fixed boundary. A distributed load from 10,000 Pa to 490,000 Pa with increment 30,000 Pa is applied on the inner surface of the diaphragm which is highlighted in Figure 25d. The remaining boundaries are set as free (not constrained) boundaries.

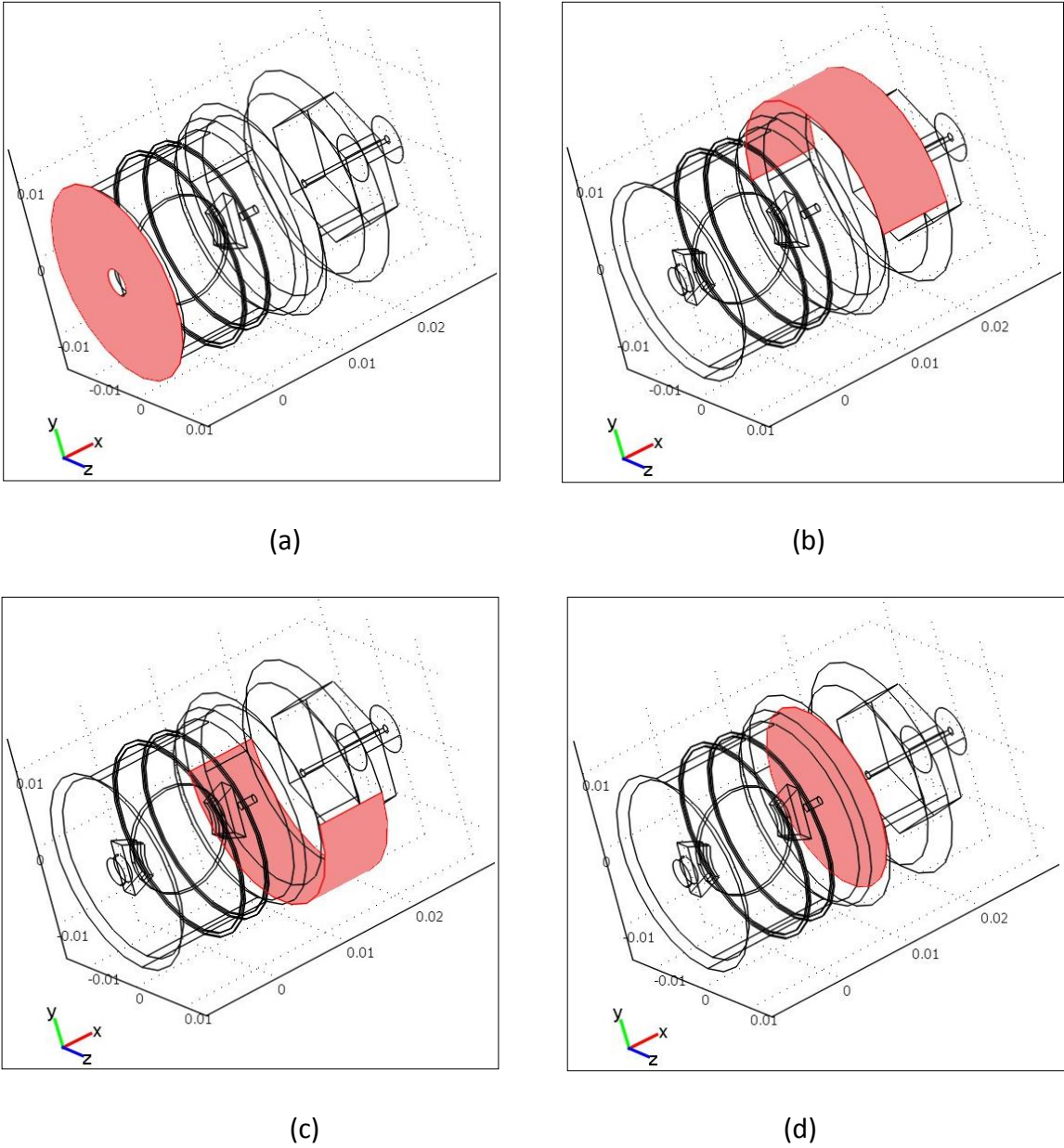


Figure 25: Boundaries (a, b, c, d) of the analyzed assembly model

After the boundary conditions are applied, the mesh analysis is performed as shown in

Figure 26.

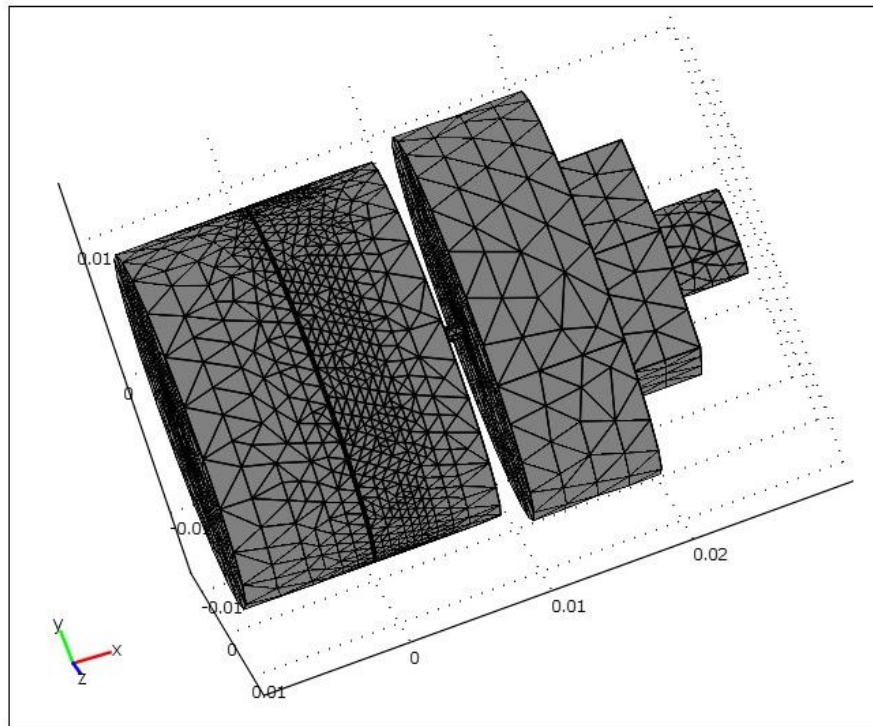


Figure 26: Mesh analysis of the analyzed assembly model

As a result of the finite element analysis, the stress on the crystal relative to the diametric dimension and the total displacement of the structure are simulated. Based on the maximum allowable force 200 N of crystal resonator, the inlet pressure of the designed pressure sensor can be determined. Figure 27 presents the FEA result of the stress distributed on the crystal along its diameter 13 mm. According to the graph, the center position ($x=0$) of the crystal has the highest stress, the stress reduces from the center to the boundary of the crystal. It is investigated that from $x=-6.5$ mm (boundary) to $x\approx-3.5$ mm and from $x\approx4.5$ mm to $x=6.5$ mm (boundary), the stress on the crystal fluctuates. This is because these two regions have the arc-shaped distributed force, which is generated when the contact surface between

the boundary of the crystal and the base of the crystal holder is an arc. Therefore, the flat surface of the crystal at the contact between the crystal and the holder is considered.

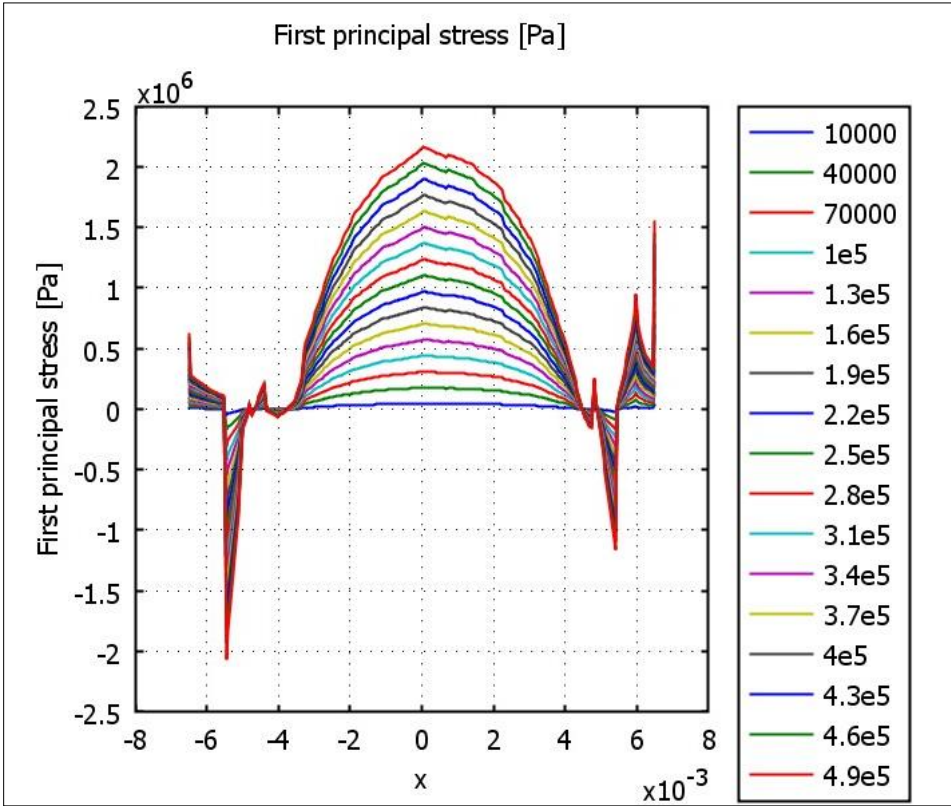


Figure 27: Stress vs. diametric dimension of the crystal resonator

As illustrated in Figure 28, the boundary and the center of the diaphragm have the highest stress. However, the stress on these positions is 41 MPa, which is much lower than yield strength of steel (250 MPa). Thus, the stress on the diaphragm is acceptable when the maximum of inlet pressure is 0.49 MPa.

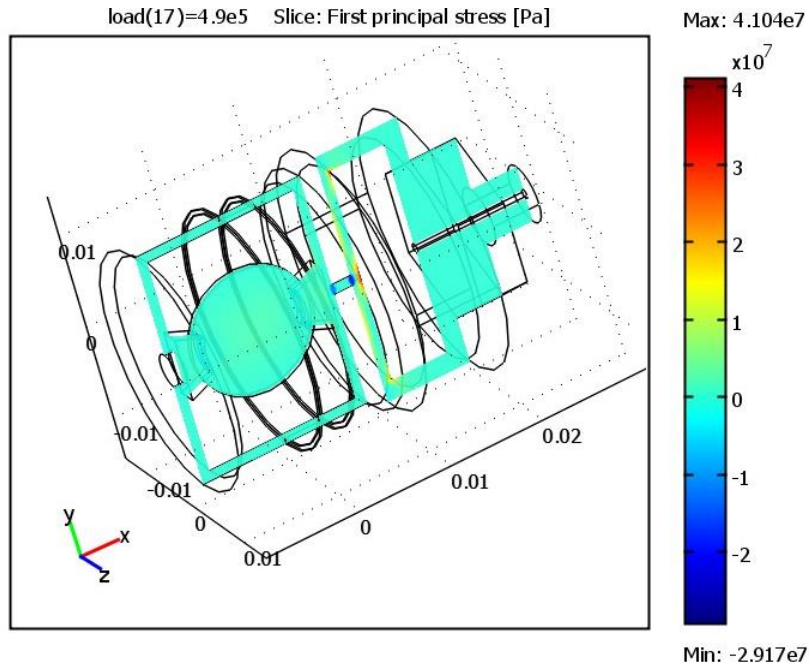


Figure 28: FEA result of stress on a diametric section of the assembly model

Figure 29 shows displacement of the assembly. The highest displacement, which is 2.086×10^{-6} m, occurs near the center of the diaphragm. Nonetheless, this value is small and acceptable.

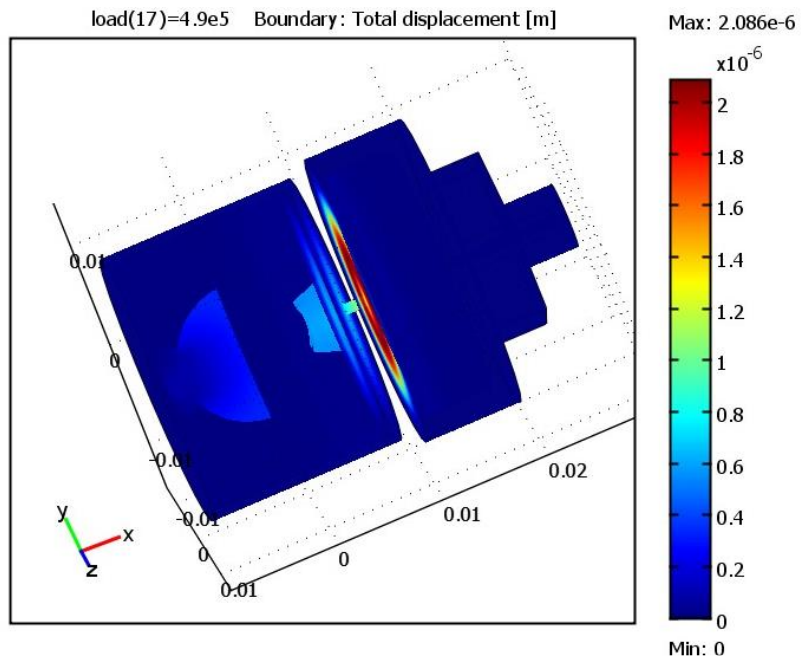


Figure 29: FEA result of displacement on the assembly model

Figure 30 demonstrates displacement on a diametric section of the assembly model. The magnitude of the displacement reduces from the diaphragm to the crystal.

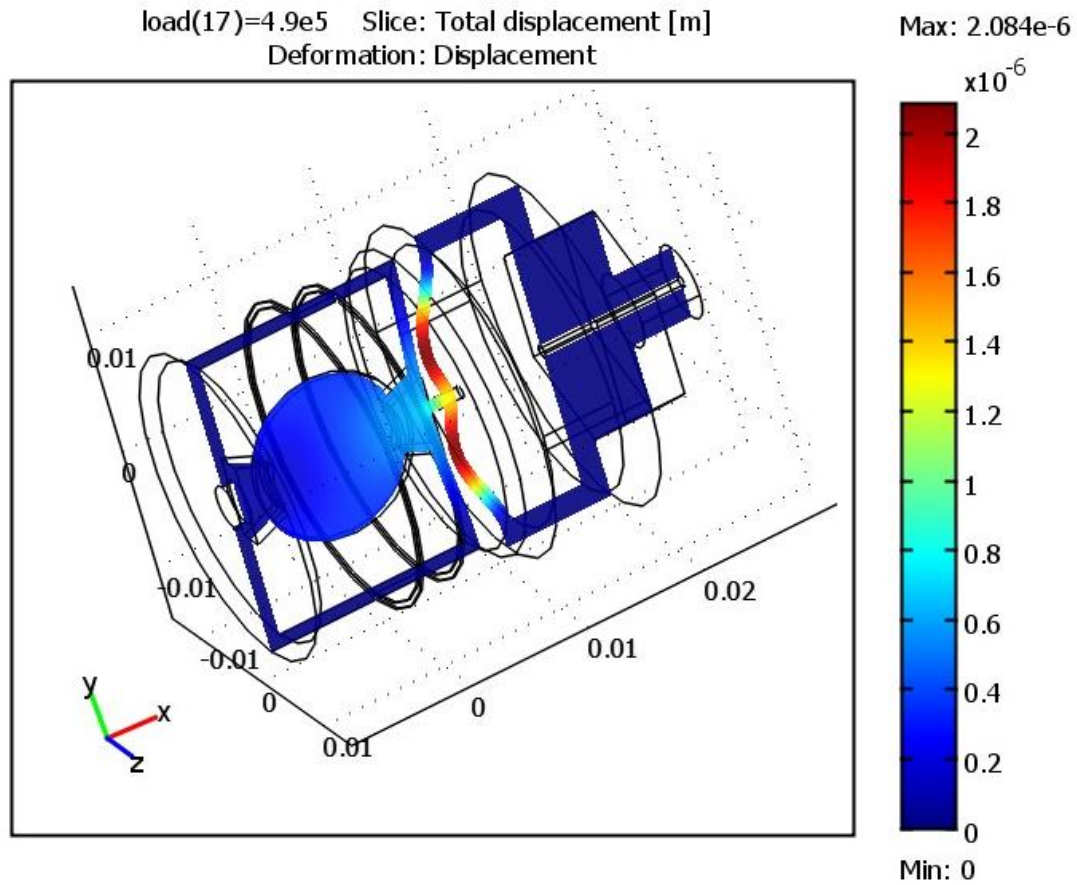


Figure 30: FEA result of displacement on a diametric section of the assembly model

Table 1 presents the data achieved from FEA on the inlet pressure and the response stress on the crystal. From the result of stress, the force applied on the crystal is calculated. Since the maximum applied force on the crystal is 200 N, based on the table 1, the corresponding maximum inlet pressure is 340,000 Pa = 49.31 Psi. The pressure value to be used in the pressure measurement experiment should be less than the maximum value considering the safety factor. Therefore, this value is 45 psi. The graph in Figure 31 represents linear relationship between the inlet pressure and force applied on the crystal.

Stress on crystal (Pa)	Pressure Inlet (Pa)	Force on crystal F (N)
44074.26	10000	5.850077443
176297.05	40000	23.4003111
308519.84	70000	40.95054475
440742.62	100000	58.50077708
572965.44	130000	76.05101472
705188.2	160000	93.60124439
837411	190000	111.1514794
969633.8	220000	128.7017144
1101856.6	250000	146.2519493
1234079.4	280000	163.8021843
1366302.1	310000	181.352406
1498525	340000	198.9026543
1630747.8	370000	216.4528893

Table 1: Maximum Force Applied on Crystal

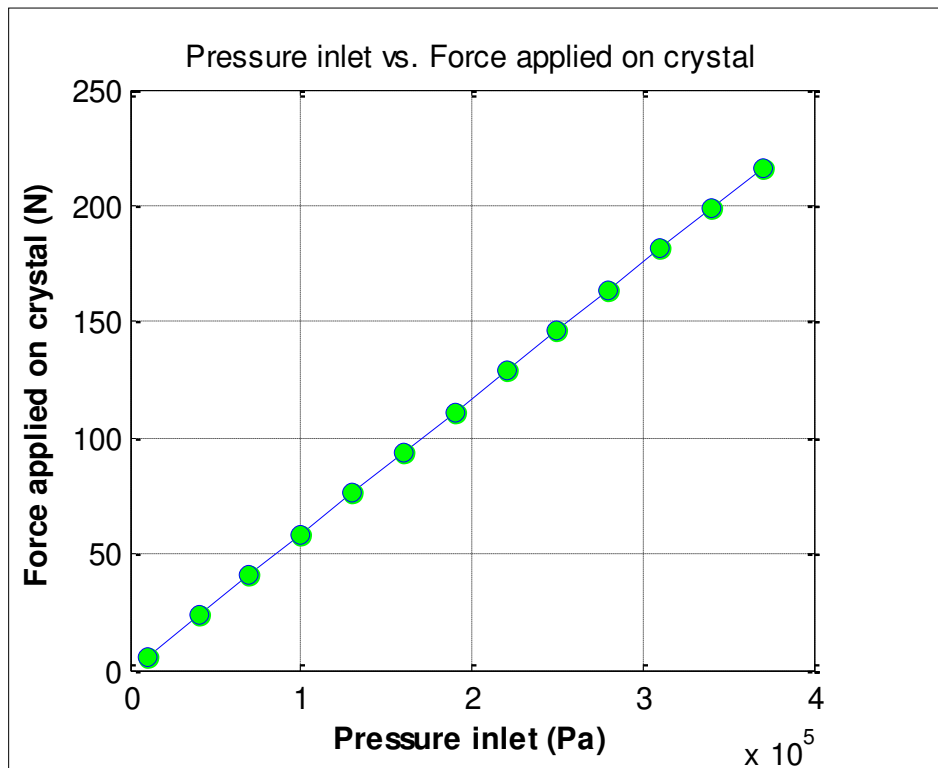


Figure 31: Linear relationship between the inlet pressure and force applied on the crystal

3.3 3D Printing Prototype

The 3D printer prototype is produced and used for the experiment before fabricating the stainless steel pressure sensor as shown in Figure 32. The material of the prototype is ABS plastic. The STL files of the 3D models are sent to 3D printer machine for manufacture. Because of the accuracy of the 3D printing machine to be used, the tolerance of the 3D models is 0.007 inch to ensure the fitness when assembling the plastic parts.

The experiment on the 3D printer prototype has been performed. The purpose of the experiment is to verify the linear relationship between applied force and the frequency output when the crystal resonator is mounted in the prototype.

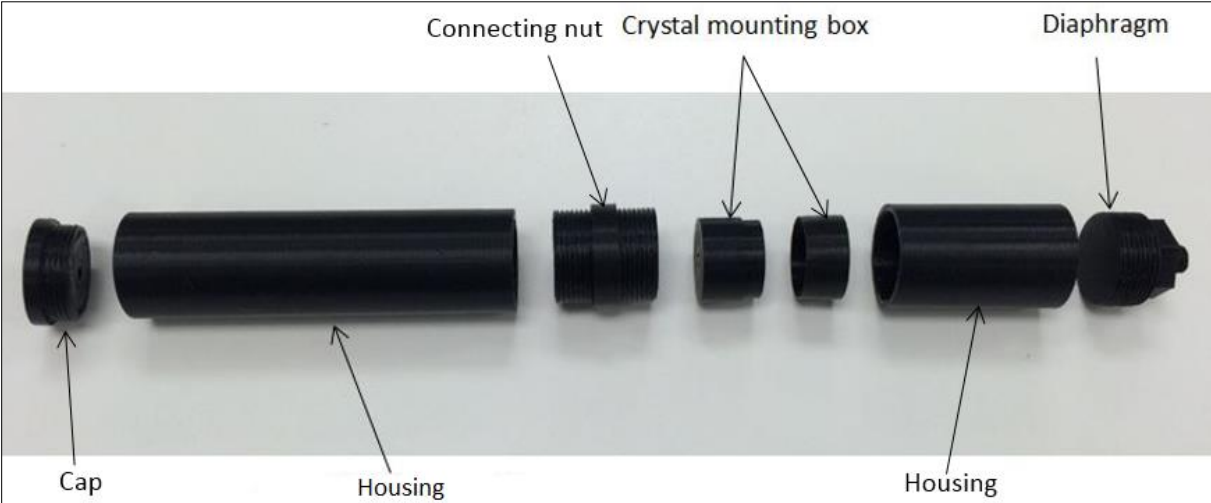


Figure 32: Prototype of the pressure sensor fabricated by a 3D printer

3.4 Experiment on 3D Printing Prototype

The crystal used in the experiment is AT-cut quartz crystal, its diameter and thickness is 13 mm and 0.66 mm relatively, and the resonance frequency is 2.5 MHz. Figure 33a shows the mounting and electrical connection of the crystal. Figure 33b indicates the fundamental frequency graph of the crystal when mounted on the two caps and before applying force. To

reduce noise, damping and yield good result, the Keysight Network Analyzer E5061B was used in the experiment. After the crystal is mounted on the box, the two electrodes are connected to Keysight NA).

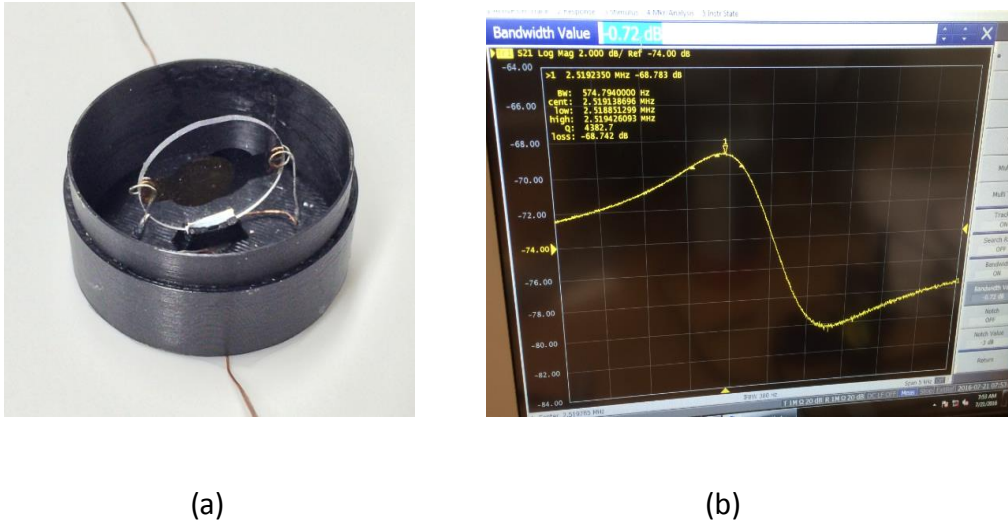


Figure 33: (a) Mounting and electrical connection of the crystal, and (b) Fundamental resonance frequency graph of the crystal when the applied force is 0 N

Figure 34a shows the connection of the crystal and the mounting of the box on the apparatus. By rotating the lead-screw, the applied force on the box is increased from 0 N to 45 N with 5 N increment. The output frequency is measured relatively by the network analyser. The force-frequency relation is found linear although this relation is not perfect (Figure 34b). Also, the frequency is increased when the applied force is increased. The imperfection of the linear relation is because of the accuracy of the manufactured prototype, the damping and noise affection. The force-frequency measurement has been repeated three times. Table 2 is the data of the applied force and response frequency of the experiment used for the graph in Figure 34b.

Force (N)	0	5	10	15	20	25	30	35	40	45
Freq. (MHz)	2.519080	2.519125	2.519156	2.519188	2.519250	2.519281	2.519313	2.519375	2.519406	2.519432

Table 2: Force-Frequency Relation

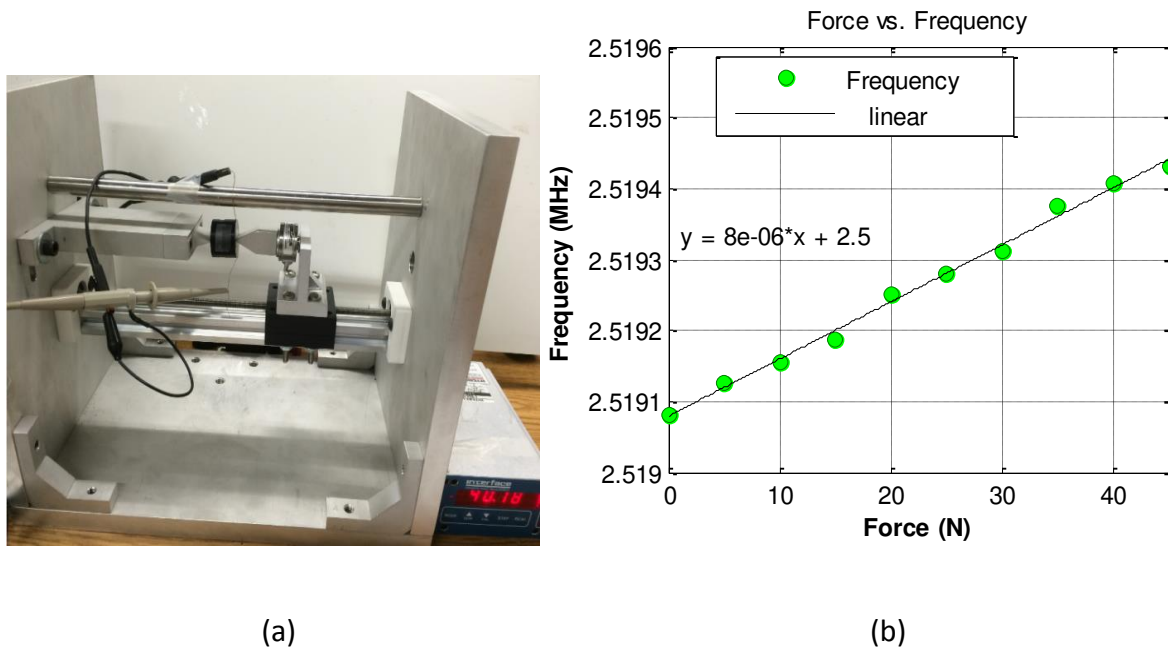


Figure 34: (a) Force applied on the box, (b) Force-frequency graph

3.5 Design and Fabrication of Pressure Sensor with Stainless Steel Housing

The material of the proposed pressure sensor is stainless steel 303 as this material has good points as mentioned previously. Figure 35 and 36 show views of the assembly of the designed pressure sensor and Figure 37 indicates a bill of material of the pressure sensor. Appendix A includes the design drawings of the pressure sensor.

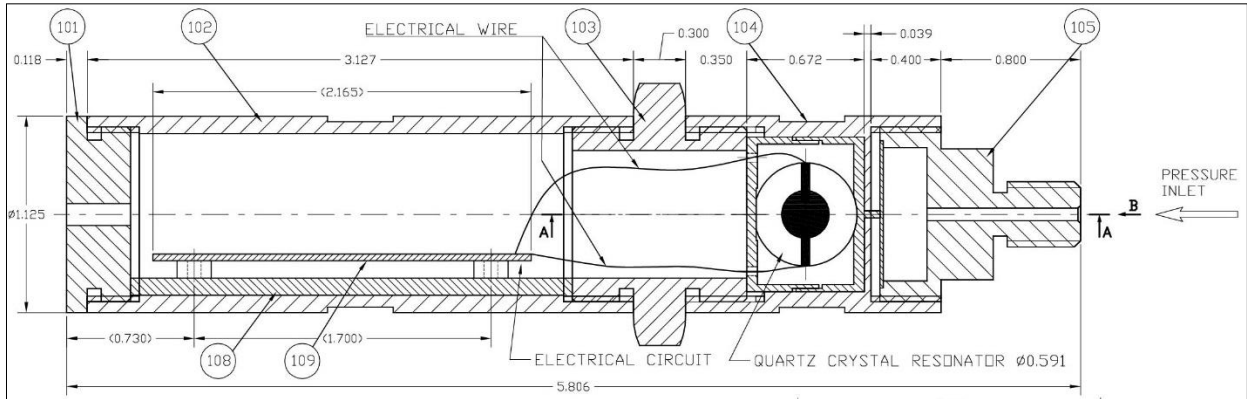


Figure 35: Section view of the assembly of the designed pressure sensor

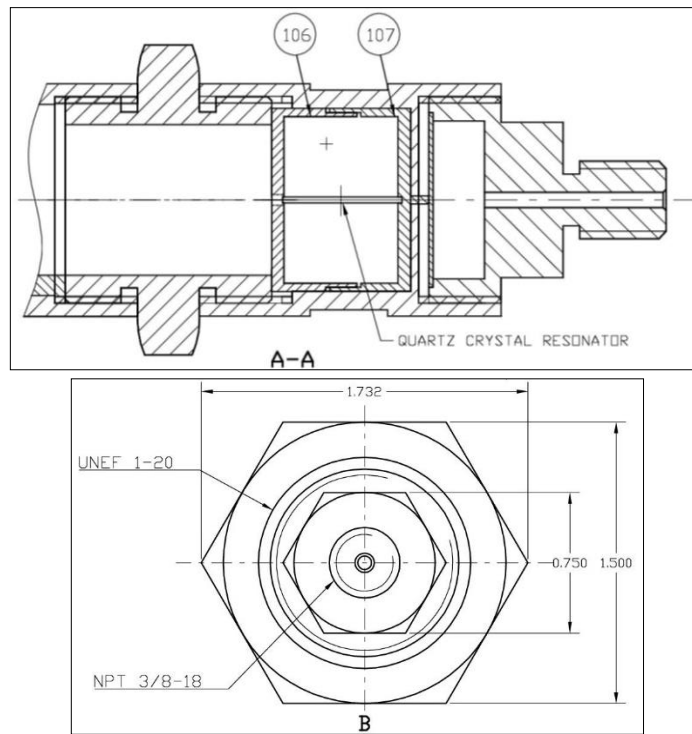


Figure 36: Detail views of the assembly of the designed pressure sensor

Item	Drawing Code, Part number	Description	Qty
101	5.01	CAP	1
102	5.02	HOUSING	1
103	5.03	NUT	1
104	5.04	HOUSING	1
105	5.05	DIAPHRAGM	1
106	5.06	CRYSTAL HOLDER	1
107	5.07	CRYSTAL HOLDER	1
108		ELECTRICAL CIRCUIT BOARD	1
109		ELECTRICAL CIRCUIT BOARD SUPPORT	1

Figure 37: Bill of material of pressure sensor assembly

As shown in Figure 38, the AT-cut quartz crystal resonator is mounted on the stainless steel lower cap, the two electrodes of the crystal are connected to electric wires by two spring coils. These wires will be connected with the designed crystal oscillator circuit.



Figure 38: Mounted crystal on one end cap (holder)

Figure 39 is the exploded view illustrating all parts of the pressure sensor. The design of the stainless steel parts are finalized and then fabricated after the FEA, 3D printing prototype, and experiments are performed. Figure 40 presents a final assembled stainless steel product.

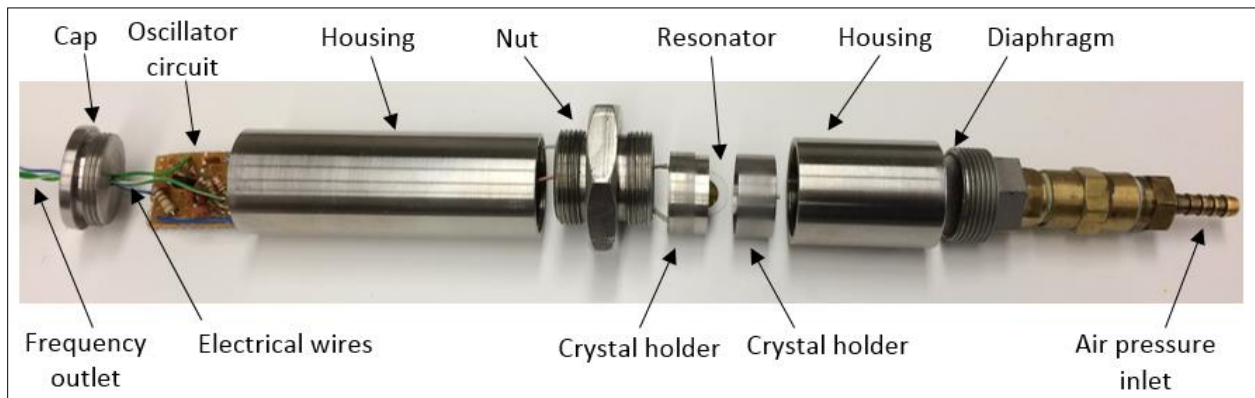


Figure 39: Stainless steel pressure sensor final assembly

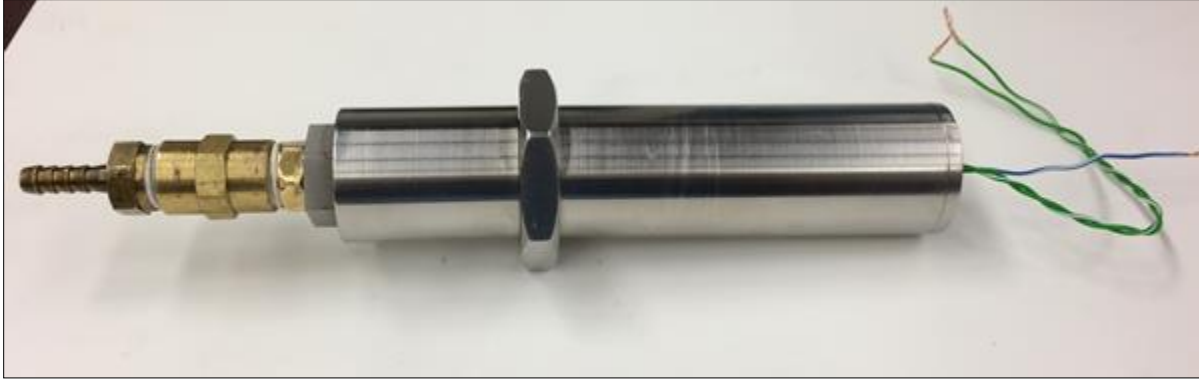


Figure 40: Final assembly of the pressure sensor with stainless steel housing

3.6 Experiment on Pressure Sensor with Stainless Steel Housing

Initially, the electrical connection and the resonance frequency of the quartz crystal resonator mounted on the lower end cap are verified from the experiment. The set up diagram of the experiment is shown in Figure 41. Figure 42 shows the frequency graph and the resonance frequency of the mounted crystal 5.26 MHz when the applied force on the crystal is 0 N.

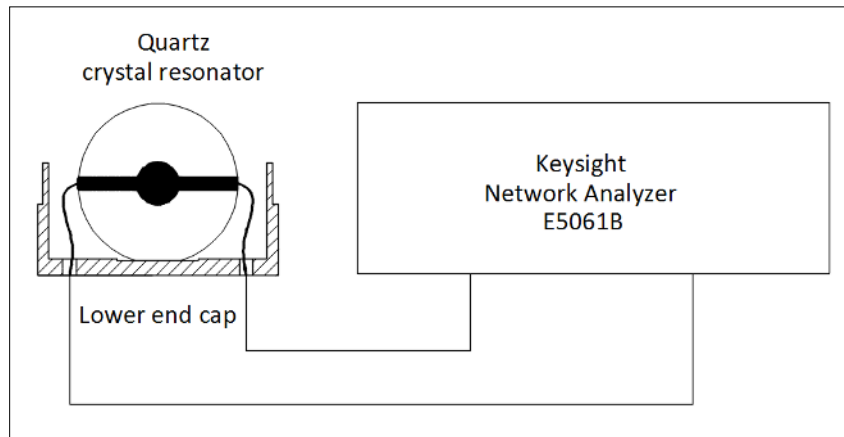


Figure 41: Diagram of the resonance frequency measurement

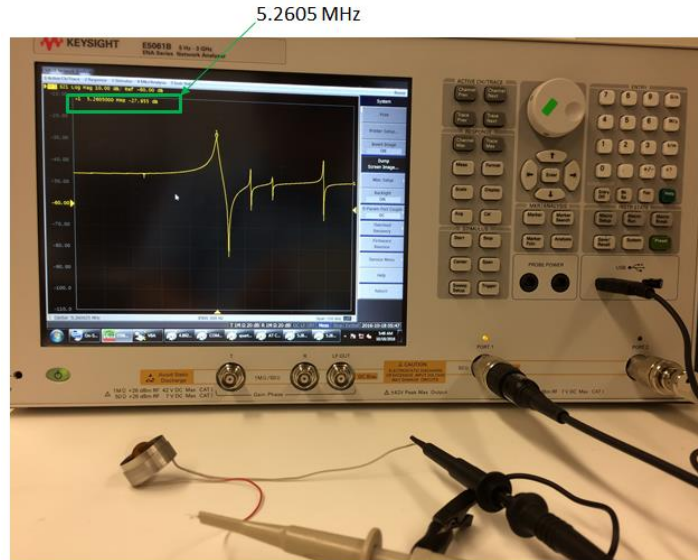


Figure 42: Resonance frequency measurement on mounted crystal

In next steps, the crystal is assembled in the mounting box and the housing for pressure testing. The inlet of the diaphragm is connected to pneumatic source. The inlet air pressure is provided from 0 psi to 45 psi with 5 psi increment. Figure 43 and 44 are schematic and pictorial diagram for the pressure measurement respectively. The input (diaphragm inlet) of the pressure sensor is connected to air pressure source and the its output is connected to the frequency counter and the oscilloscope to check the resonance frequency shift and the graph of the sine wave form of the relative frequency. The pressure sensor is supplied with 3.7 VDC. This means the input of the oscillator circuit of the pressure sensor is connected to 3.7 VDC.

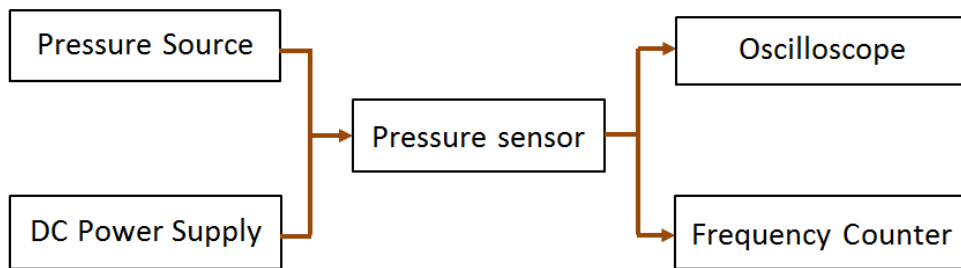


Figure 43: Schematic diaphragm of the pressure measurement experiment setup

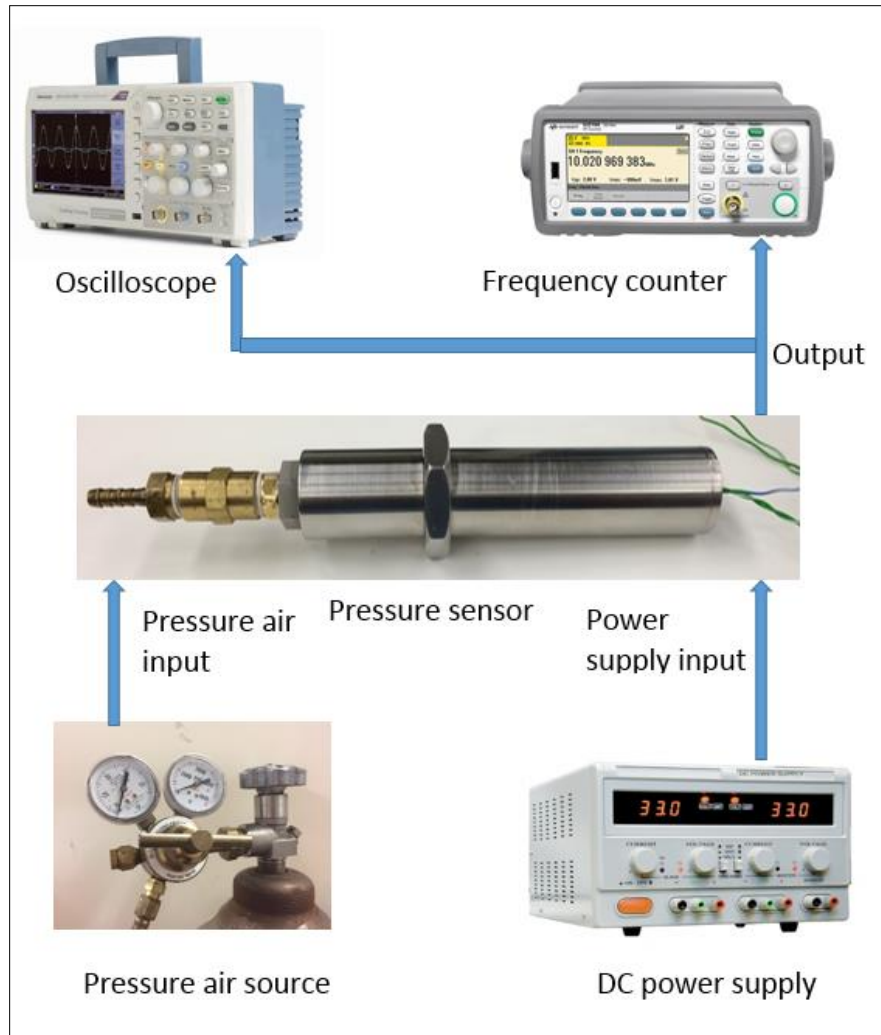


Figure 44: Pictorial diagram of the pressure measurement experiment setup

Figure 45 shows a sine wave form of the output on the oscilloscope and the relative resonance frequency on the frequency counter. The crystal resonator is connected to the circuit as illustrated in Figure 46.

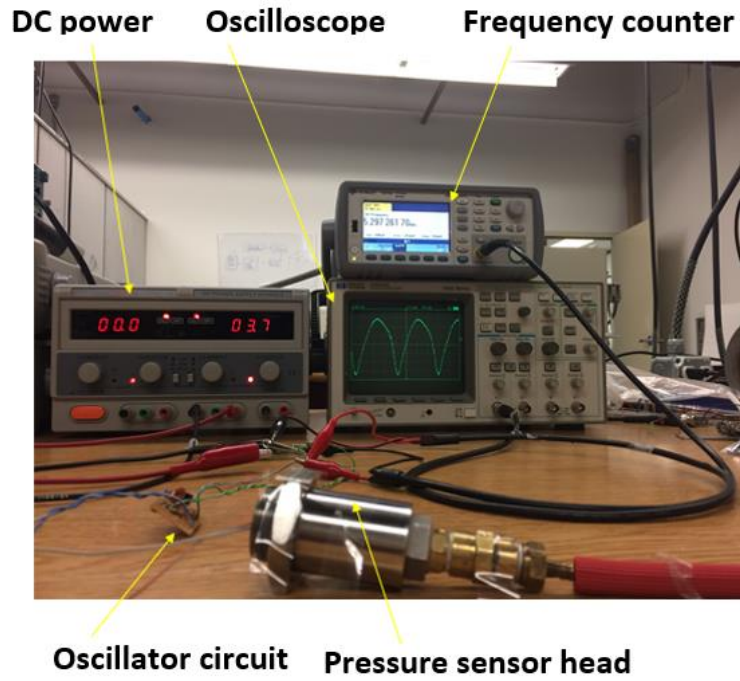


Figure 45: Pressure measurement experiment and graph result

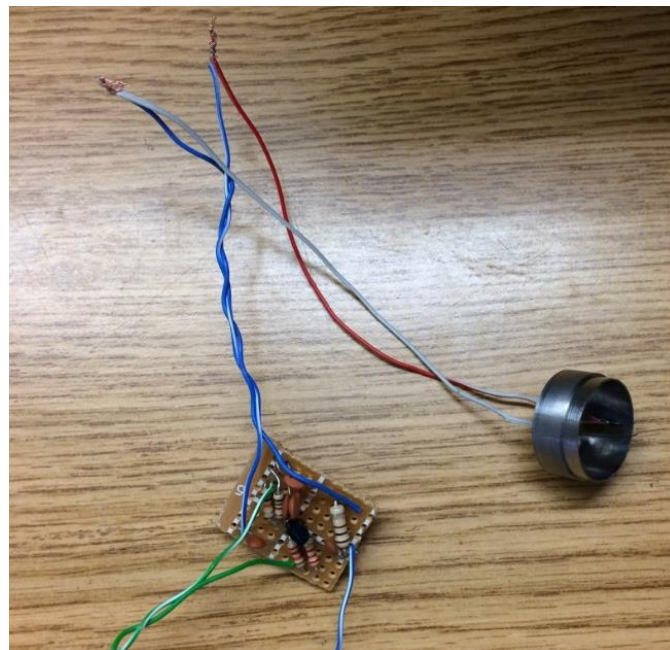


Figure 46: Fabricated crystal oscillator circuit

The graph in Figure 47 is the result of the pressure measurement experiment on the pressure sensor. The graph shows good linear relationship between the inlet (pressure) and the outlet (frequency).

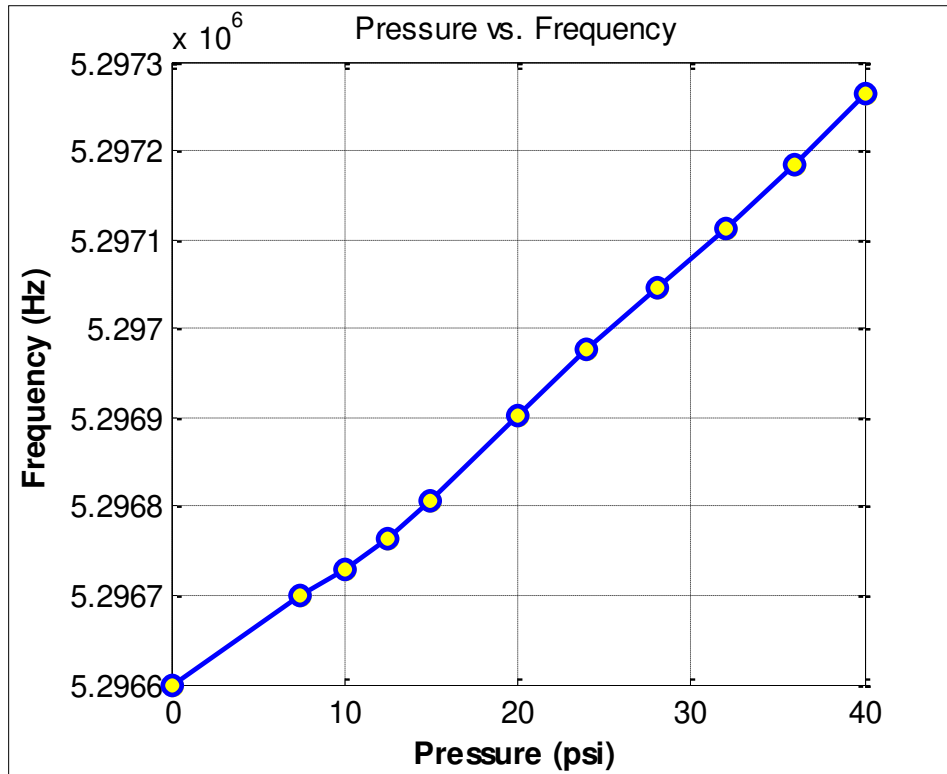


Figure 47: Pressure measurement result of the designed pressure sensor

3.7 Crystal Oscillator Circuit Design

Dual-mode crystal resonator circuit probes the resonator with the superposition of two harmonic modes simultaneously. It excites crystal resonator in fundamental mode and third overtone mode [37]. The thesis focuses on the circuit that can excite the crystal resonator in fundamental harmonic mode and experiments based on this circuit. The crystal oscillator circuit is designed to excite the AT-cut quartz crystal resonator at its fundamental resonance frequency and send the frequency signal to the output of the circuit. The input power supply

for the circuit is +15 VDC. The electrical components are available and common commercial parts. Figure 48 and 49 describe the details of the designed crystal oscillator circuit and the fabricated circuit relatively.

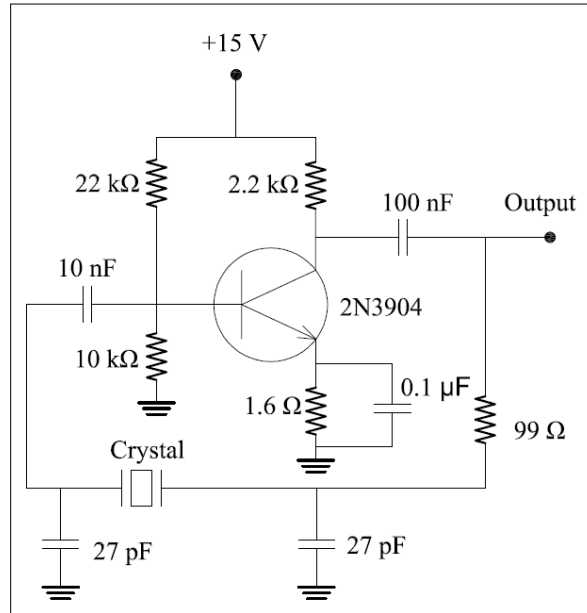


Figure 48: Designed crystal oscillator circuit

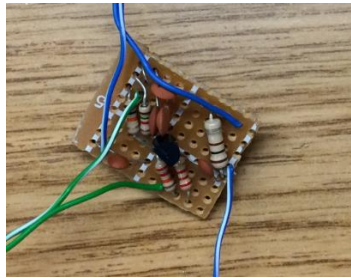


Figure 49: Fabricated crystal oscillator circuit

3.8 Beat Frequency Experiment

As aforementioned, the beat frequency is between the fundamental frequency and the third overtone frequency. Researches show that the relationship between the beat frequency and the temperature is linear. Therefore, the temperature compensation in pressure measurement can be enabled based on the beat frequency and temperature relation and the

microprocessor. In this research, the experiments on the beat frequency vs. temperature on AT-cut quartz and LGS crystal resonator are performed.

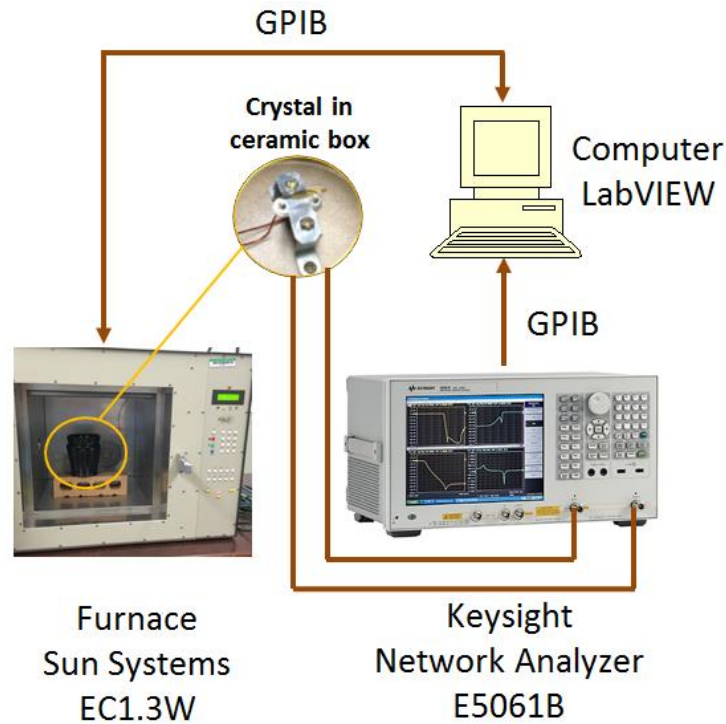


Figure 50: Diagram of the experiment setup on temperature vs. frequency

Figure 50 shows a diagram of the experiment setup for the temperature vs. frequency measurement and Figure 51 presents photos of the experiment. A furnace, KEYSIGHT E5016B network analyzer, and LabVIEW on computer are connected through GPIB. The air flow in the furnace can influence the measurement result when the flow contacts the crystal resonator directly. For this reason, the crystal is mounted inside a ceramic box as shown in Figure 52 to minimize the influence of the air flow.

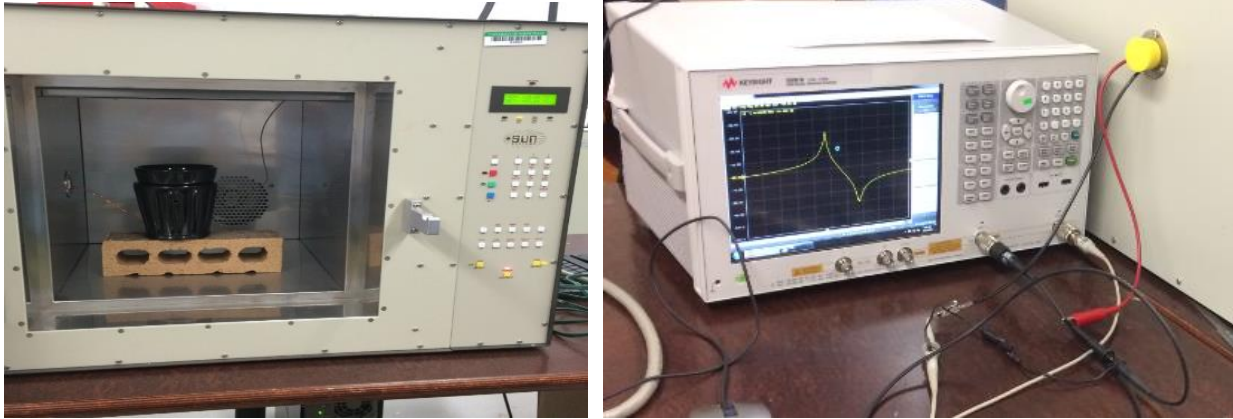


Figure 51: Photos of the experiment set up for beat frequency vs. temperature



Figure 52: Crystal resonator mounting and connection in the ceramic box

In the experiment, the frequency vs. temperature relation of quartz and LGS are measured at 1st and then 3rd harmonic mode of vibration. The temperature inside the furnace is increased from room temperature to 50°C . The LabVIEW program controls the temperature and records the data of temperature and resonance frequency of the crystal. Also, the LabVIEW controlled network analyzer program tracks the resonance frequency variation of the crystal and yields a graph of resonance frequency vs. temperature.

The resonance frequency variation with respect to the temperature of quartz and LGS excited at first and third overtone are given in Figure 53 and 54 respectively. In quartz, the difference of the temperature vs. frequency relation graph between first and third overtone is explicitly seen. When the quartz crystal is excited at first overtone (fundamental vibration mode), the slope of the temperature vs. frequency is positive. In contrast, the slope is negative in third overtone (3 times fundamental frequency).

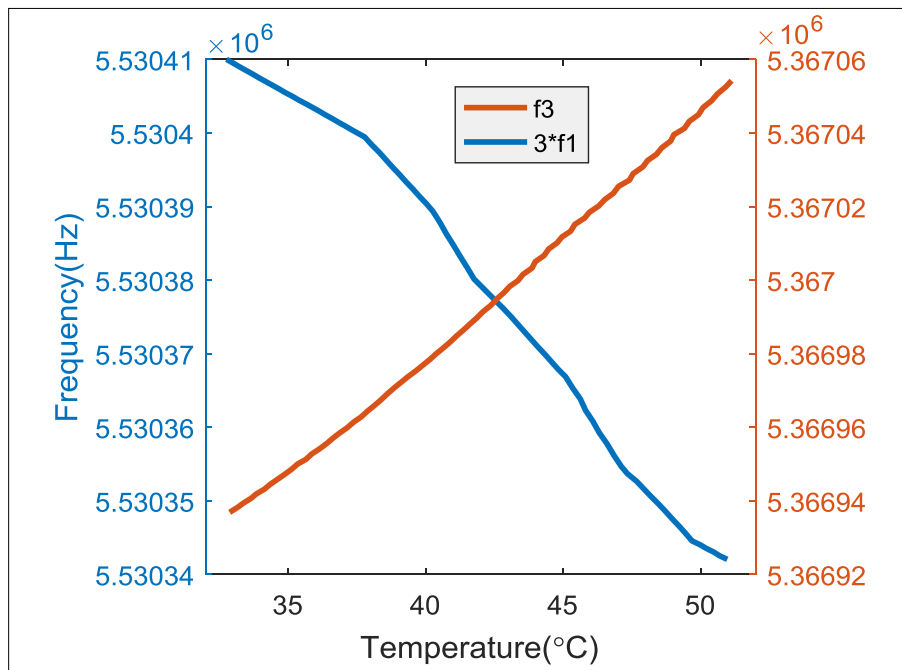


Figure 53: 3*fundamental frequency and 3rd overtone frequency vs. temperature in quartz

In LGS, the difference of the temperature vs. frequency relation graph between first and third overtone is not as clear as that of quartz as shown in Figure 54.

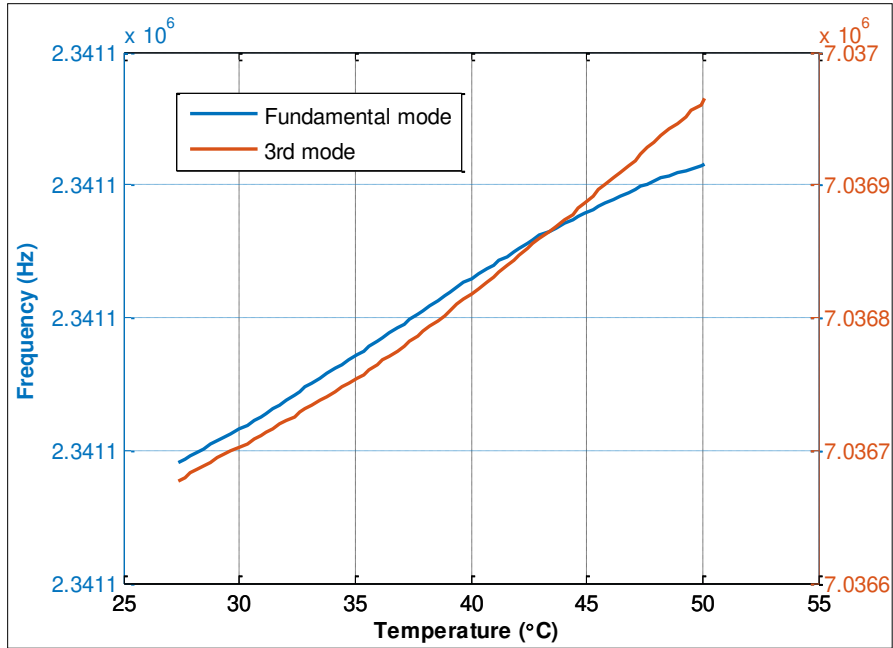


Figure 54: 3* fundamental frequency and 3rd overtone frequency vs. temperature in LGS

The beat frequency variation with respect to temperature of quartz and LGS are calculated and the graphs are drawn as described in Figure 55 and 56 respectively. From the results, the linear relationship between beat frequency and temperature in quartz is verified. Whereas, the relationship is not linear in LGS.

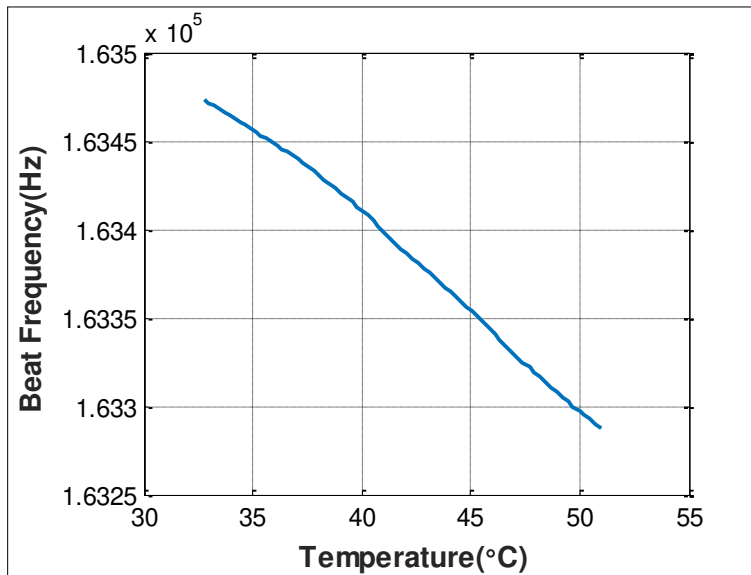


Figure 55: Beat frequency vs. temperature of quartz

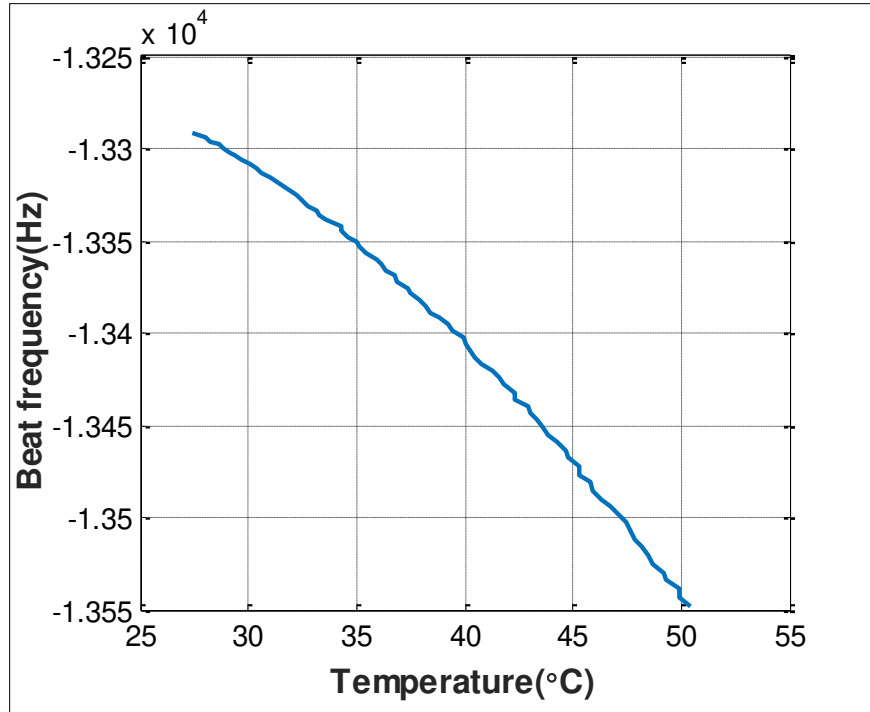


Figure 56: Beat frequency vs. temperature of LGS

With the linear relationship found in quartz as shown in Figure 55, the temperature compensation for the pressure measurement of quartz based pressure sensor can be performed.

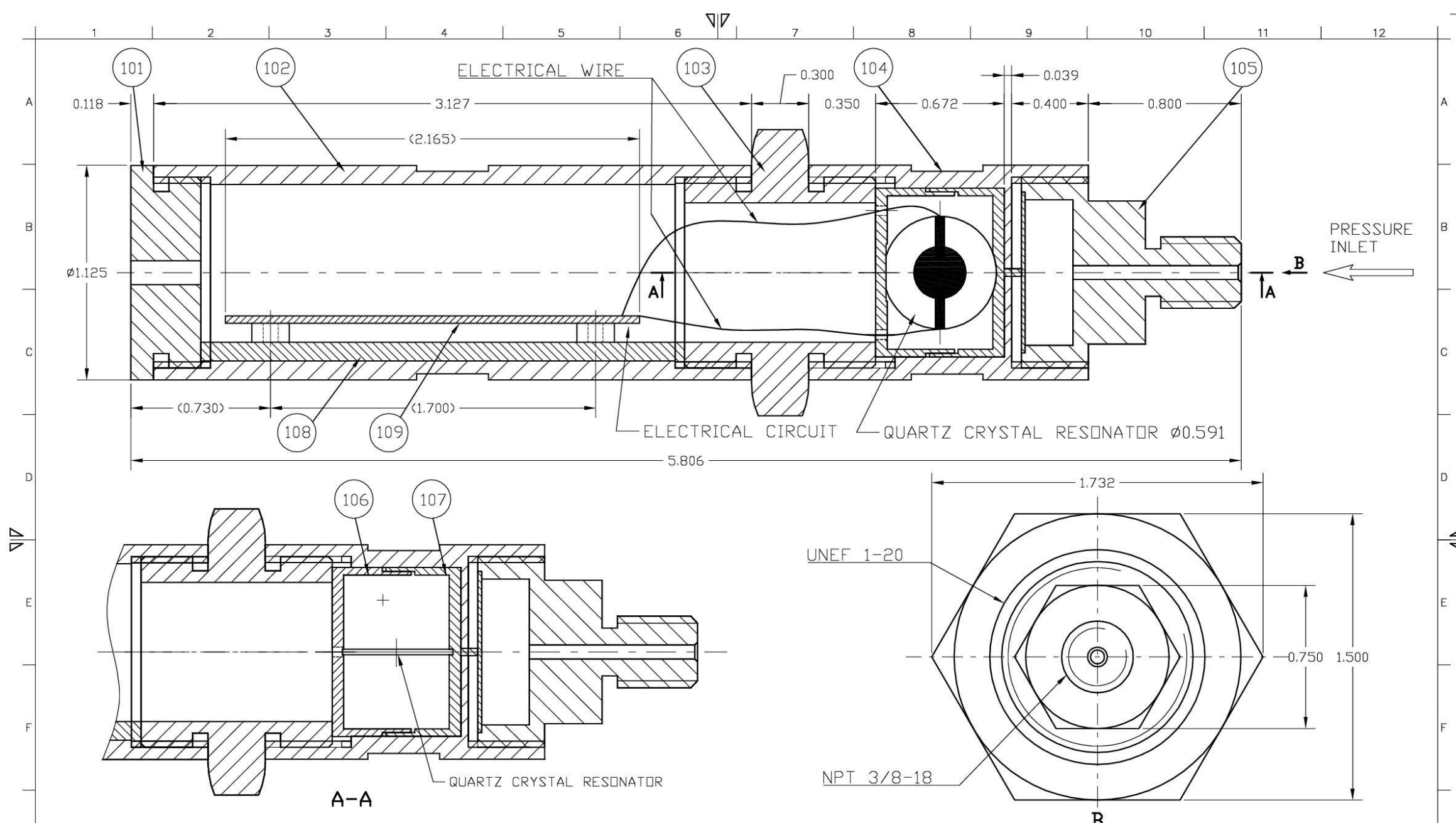
CHAPTER 4

CONCLUSION AND FUTURE RESEARCH

The design, modeling, and experiment of a novel pressure sensor using a dual-mode AT-cut quartz crystal resonator with beat frequency analysis based temperature compensation technique have been accomplished. The combination of a compact design of the proposed piezo crystal resonator structure and temperature compensation technique gives advantages such as high accuracy, low cost, and good performance attributes. The use of a single dual-mode crystal resonator to measure force and temperature simultaneously minimizes the thermal lag problem which affects the accuracy of the pressure measurement. The FEA (Finite Element Analysis) of the diaphragm and the crystal resonator are performed to verify the design. A 3D printing prototype of the pressure sensor has been fabricated, and its performance is verified through a force-frequency effect experiment using a designed apparatus. In addition, a stainless steel pressure sensor and a crystal oscillator circuit have been fabricated. The pressure measurement experiment performed on the stainless steel sensor shows a good linear relationship between the input (pressure) and the output (frequency). Future researches are the design and experiments on the all-LGS structure based pressure sensor at high temperatures to find out the performance of this sensor at high temperatures.

APPENDIX A

DESIGN DRAWINGS OF PRESSURE SENSOR



BILL OF MATERIAL:

Item	Drawing Code, Part number	Description	Qty
101	5.01	CAP	1
102	5.02	HOUSING	1
103	5.03	NUT	1
104	5.04	HOUSING	1
105	5.05	DIAPHRAGM	1
106	5.06	CRYSTAL HOLDER	1
107	5.07	CRYSTAL HOLDER	1
108		ELECTRICAL CIRCUIT BOARD	1
109		ELECTRICAL CIRCUIT BOARD SUPPORT	1

ALL DIMENSIONS ARE IN INCHES.

UNIVERSITY OF NORTH TEXAS, ETEC

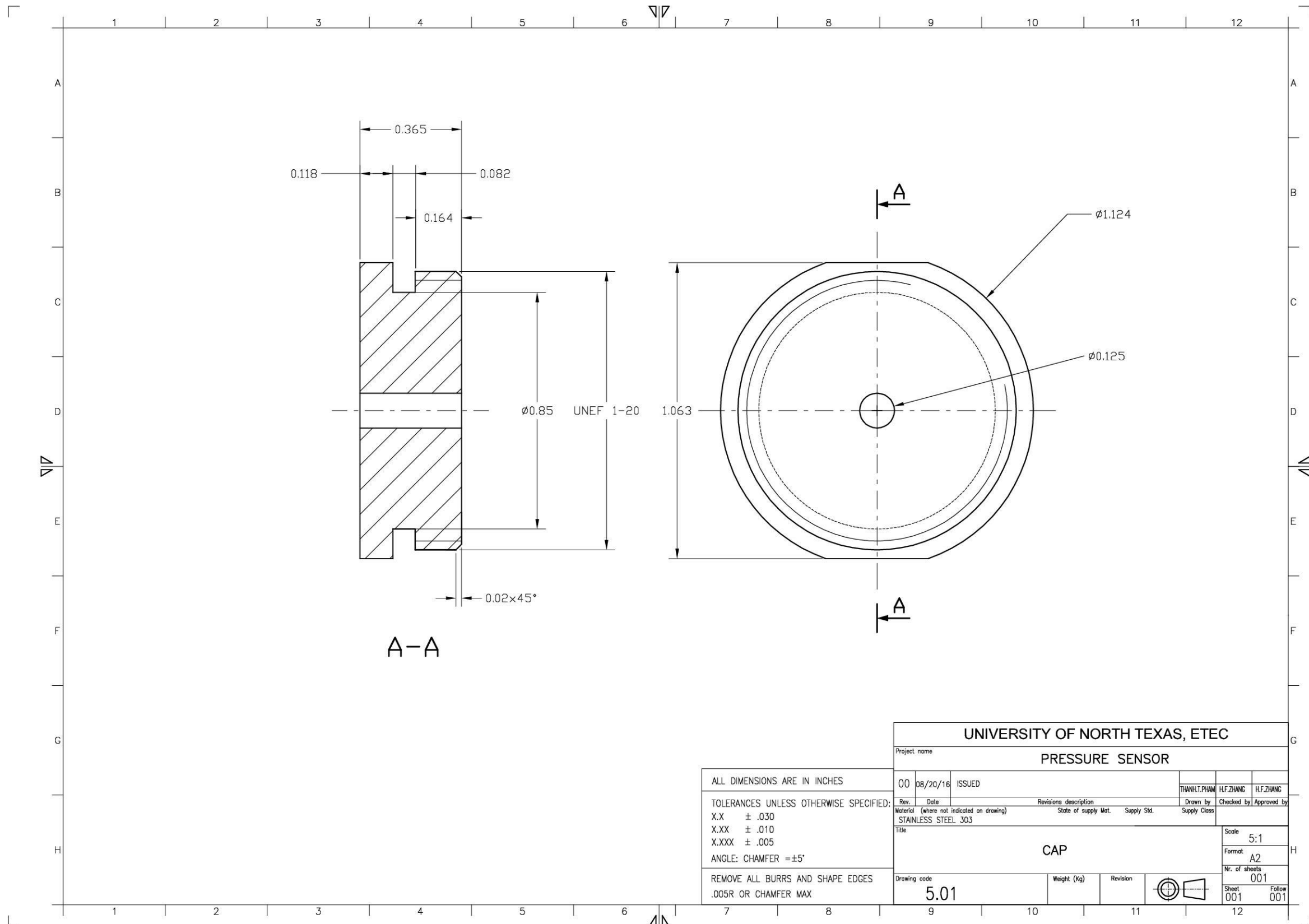
Project name: **PRESSURE SENSOR**

00	08/20/16	ISSUED	THANH.T.PHAM	H.F.ZHANG	H.F.ZHANG
Date	Revisions description	Drawn by	Checked by	Approved by	
Material (where not indicated on drawing)		State of supply Mat.	Supply Std.	Supply Class	

PRESSURE SENSOR WITH CRYSTAL RESONATOR

Scale: 3:1
Format: A2
N. of sheets: 001
Sheet: 001 Follow: 001

Weight (Kg): 8.01

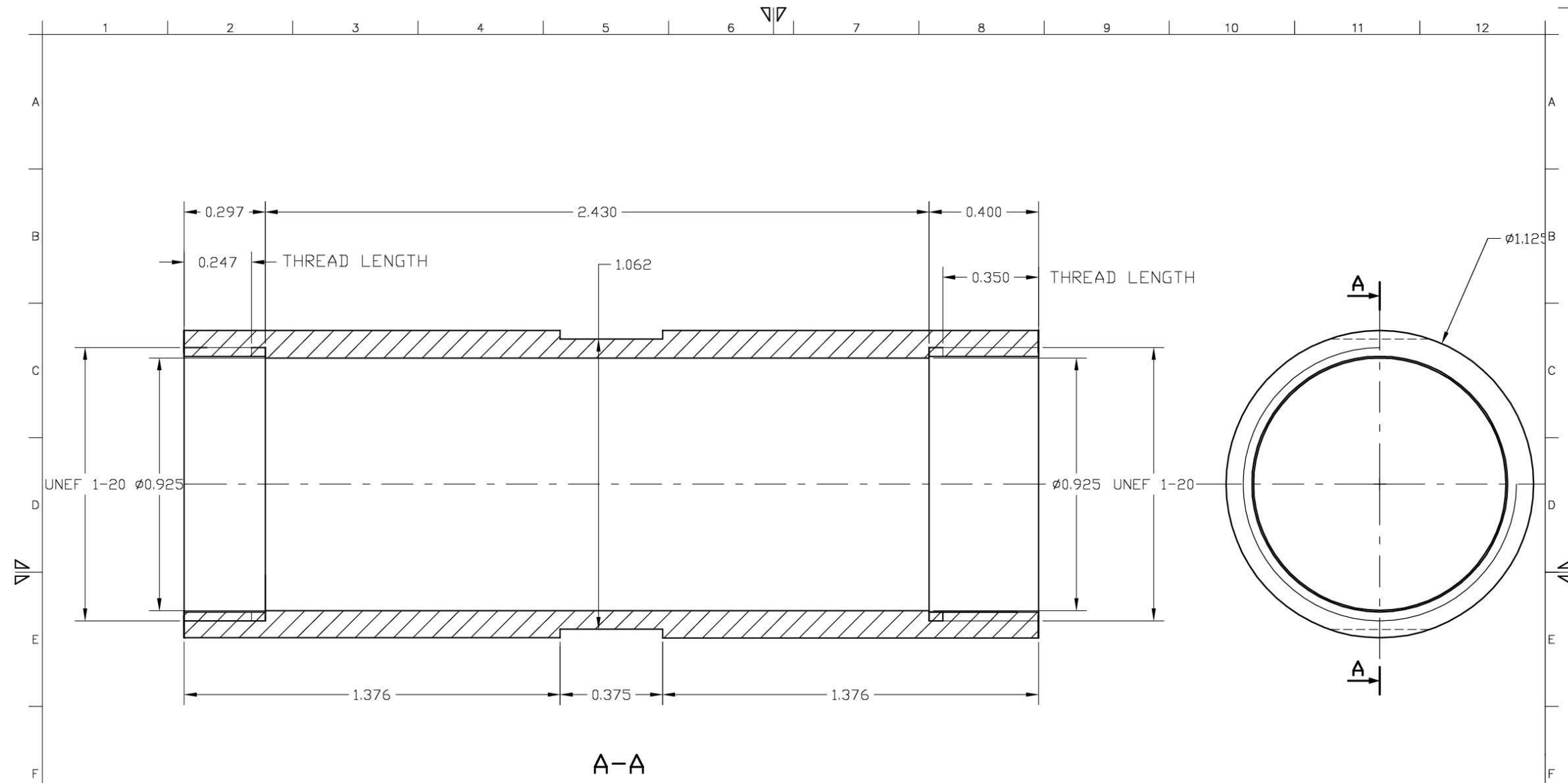


A-A

UNIVERSITY OF NORTH TEXAS, ETEC

Project name: PRESSURE SENSOR

00	08/20/16	ISSUED	THANH.T.PHAM	H.F.ZHANG	H.F.ZHANG
TOLERANCES UNLESS OTHERWISE SPECIFIED:		Material (where not indicated on drawing)			
X.X	± .030	STAINLESS STEEL 303			
X.XX	± .010	Title			
X.XXX	± .005	CAP			
ANGLE: CHAMFER =±5°		Scale: 5:1			
REMOVE ALL BURRS AND SHAPE EDGES		Format: A2			
.005R OR CHAMFER MAX		Nr. of sheets: 001			
Drawing code: 5.01		Sheet: 001			
		Follow: 001			



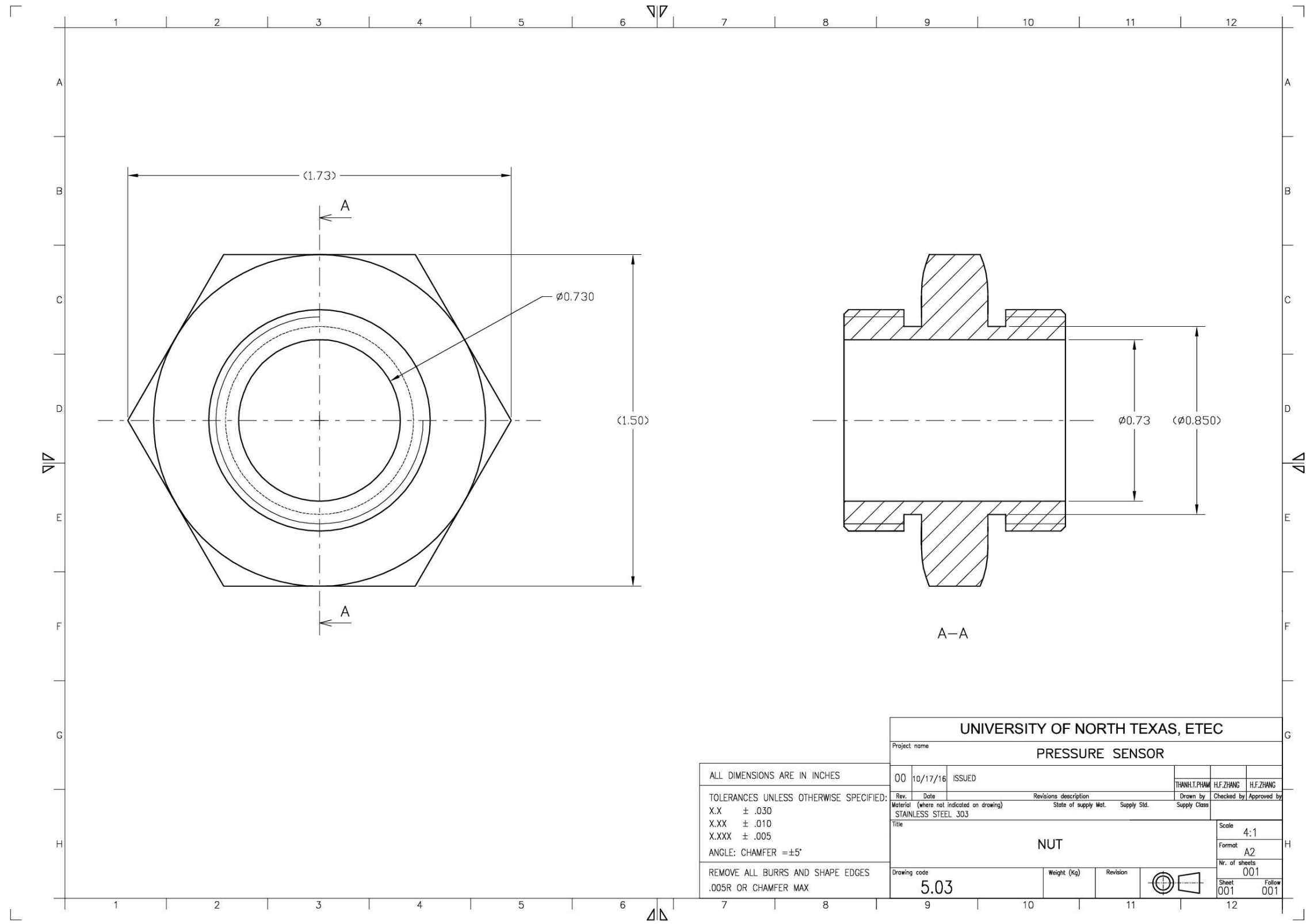
ALL DIMENSIONS ARE IN INCHES

TOLERANCES UNLESS OTHERWISE SPECIFIED:
 X.X ± .030
 X.XX ± .010
 X.XXX ± .005

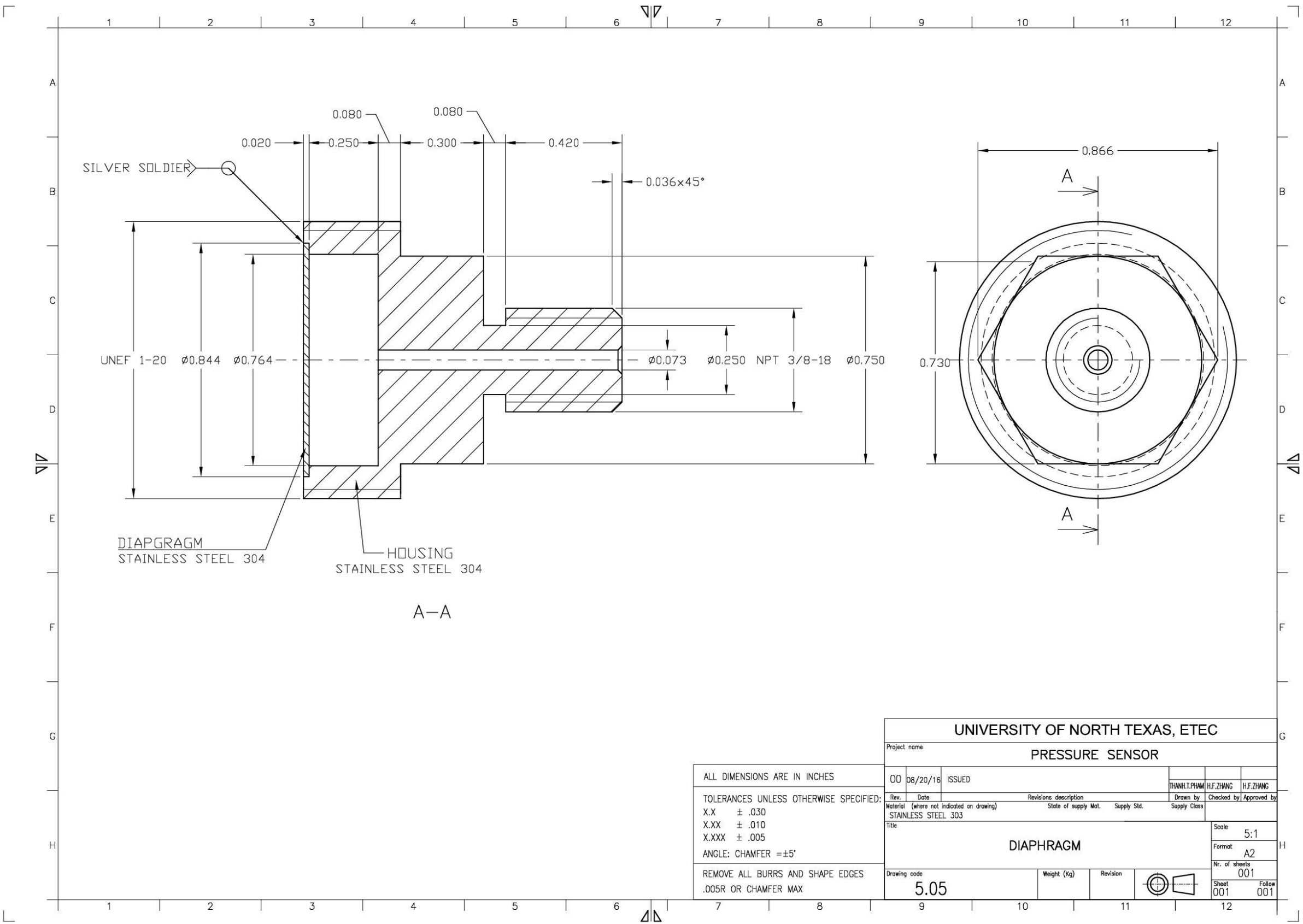
ANGLE: CHAMFER = ±5°

REMOVE ALL BURRS AND SHAPE EDGES
 .005R OR CHAMFER MAX

UNIVERSITY OF NORTH TEXAS, ETEC					
Project name					
PRESSURE SENSOR					
00	08/20/16	ISSUED	THANH.T.PHAM	H.F.ZHANG	H.F.ZHANG
Rev.	Date	Revisions description	Drawn by	Checked by	Approved by
Material (where not indicated on drawing)			State of supply Mat.	Supply Std.	Supply Class
STAINLESS STEEL 303					
Title				Scale	4:1
HOUSING				Format	A2
Drawing code				Nr. of sheets	001
5.02		Weight (Kg)	Revision	Sheet	001
				Follow	001



UNIVERSITY OF NORTH TEXAS, ETEC																																																																																																											
Project name: PRESSURE SENSOR																																																																																																											
<table border="1" style="width: 100%; border-collapse: collapse;"> <tr> <td style="width: 15%;">ALL DIMENSIONS ARE IN INCHES</td> <td style="width: 5%;">00</td> <td style="width: 10%;">10/17/16</td> <td style="width: 15%;">ISSUED</td> <td style="width: 10%;"></td> <td style="width: 10%;"></td> <td style="width: 10%;"></td> <td style="width: 10%;"></td> <td style="width: 10%;"></td> <td style="width: 10%;"></td> </tr> <tr> <td>TOLERANCES UNLESS OTHERWISE SPECIFIED:</td> <td>Rev.</td> <td>Date</td> <td>Revisions description</td> <td>Drawn by</td> <td>Checked by</td> <td>Approved by</td> <td colspan="4"></td> </tr> <tr> <td>X.X ± .030</td> <td></td> <td></td> <td></td> <td></td> <td></td> <td></td> <td>Material (where not indicated on drawing)</td> <td>State of supply Mat.</td> <td>Supply Std.</td> <td>Supply Class</td> </tr> <tr> <td>X.XX ± .010</td> <td></td> <td></td> <td></td> <td></td> <td></td> <td></td> <td colspan="4">STAINLESS STEEL 303</td> </tr> <tr> <td>X.XXX ± .005</td> <td colspan="10">Title: NUT</td> </tr> <tr> <td>ANGLE: CHAMFER =±5°</td> <td colspan="10">Scale: 4:1</td> </tr> <tr> <td>REMOVE ALL BURRS AND SHAPE EDGES</td> <td colspan="10">Format: A2</td> </tr> <tr> <td>.005R OR CHAMFER MAX</td> <td colspan="10">Nr. of sheets: 001</td> </tr> <tr> <td></td> <td colspan="2">Drawing code: 5.03</td> <td colspan="2">Weight (Kg)</td> <td colspan="2">Revision</td> <td colspan="2">Sheet: 001</td> <td colspan="2">Follow: 001</td> </tr> </table>										ALL DIMENSIONS ARE IN INCHES	00	10/17/16	ISSUED							TOLERANCES UNLESS OTHERWISE SPECIFIED:	Rev.	Date	Revisions description	Drawn by	Checked by	Approved by					X.X ± .030							Material (where not indicated on drawing)	State of supply Mat.	Supply Std.	Supply Class	X.XX ± .010							STAINLESS STEEL 303				X.XXX ± .005	Title: NUT										ANGLE: CHAMFER =±5°	Scale: 4:1										REMOVE ALL BURRS AND SHAPE EDGES	Format: A2										.005R OR CHAMFER MAX	Nr. of sheets: 001											Drawing code: 5.03		Weight (Kg)		Revision		Sheet: 001		Follow: 001	
ALL DIMENSIONS ARE IN INCHES	00	10/17/16	ISSUED																																																																																																								
TOLERANCES UNLESS OTHERWISE SPECIFIED:	Rev.	Date	Revisions description	Drawn by	Checked by	Approved by																																																																																																					
X.X ± .030							Material (where not indicated on drawing)	State of supply Mat.	Supply Std.	Supply Class																																																																																																	
X.XX ± .010							STAINLESS STEEL 303																																																																																																				
X.XXX ± .005	Title: NUT																																																																																																										
ANGLE: CHAMFER =±5°	Scale: 4:1																																																																																																										
REMOVE ALL BURRS AND SHAPE EDGES	Format: A2																																																																																																										
.005R OR CHAMFER MAX	Nr. of sheets: 001																																																																																																										
	Drawing code: 5.03		Weight (Kg)		Revision		Sheet: 001		Follow: 001																																																																																																		



DIAPHRAGM
STAINLESS STEEL 304

HOUSING
STAINLESS STEEL 304

A-A

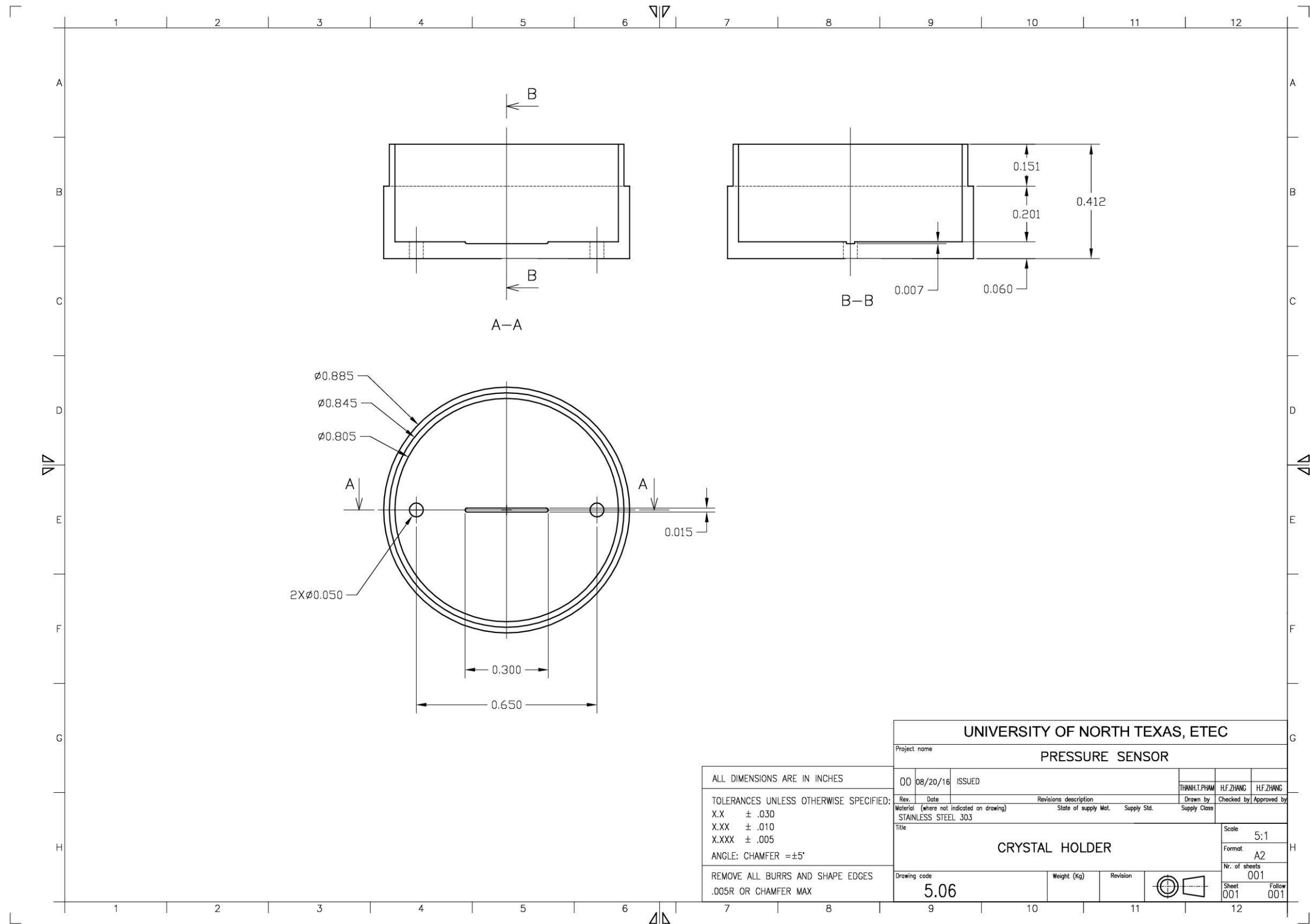
ALL DIMENSIONS ARE IN INCHES

TOLERANCES UNLESS OTHERWISE SPECIFIED:
 X.X ± .030
 X.XX ± .010
 X.XXX ± .005

ANGLE: CHAMFER = ±5°

REMOVE ALL BURRS AND SHAPE EDGES
 .005R OR CHAMFER MAX

UNIVERSITY OF NORTH TEXAS, ETEC					
Project name PRESSURE SENSOR					
00	08/20/16	ISSUED	THANH.T.PHAM	H.F.ZHANG	H.F.ZHANG
Rev.	Date	Revisions description	Drawn by	Checked by	Approved by
Material (where not indicated on drawing) STAINLESS STEEL 303			State of supply Mat.	Supply Std.	Supply Class
Title DIAPHRAGM				Scale	5:1
				Format	A2
				Nr. of sheets	001
Drawing code 5.05		Weight (Kg)	Revision	Sheet 001	Follow 001



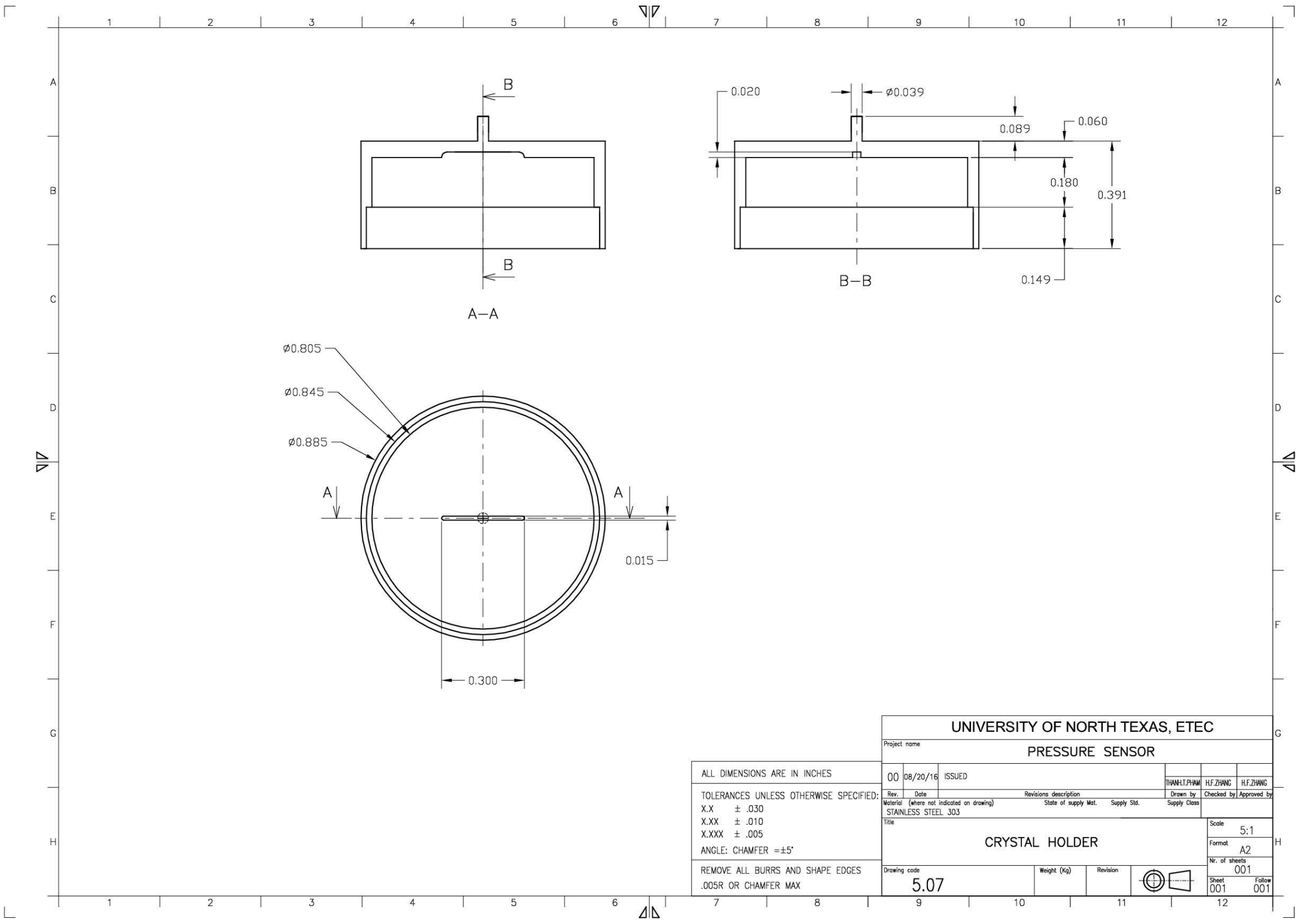
ALL DIMENSIONS ARE IN INCHES

TOLERANCES UNLESS OTHERWISE SPECIFIED:
 X.X ± .030
 X.XX ± .010
 X.XXX ± .005

ANGLE: CHAMFER = ±5°

REMOVE ALL BURRS AND SHAPE EDGES
 .005R OR CHAMFER MAX

UNIVERSITY OF NORTH TEXAS, ETEC					
Project name					
PRESSURE SENSOR					
Rev.	Date	Revisions description	Drawn by	Checked by	Approved by
00	08/20/16	ISSUED	THANH.T.PHAM	H.F.ZHANG	H.F.ZHANG
Material (where not indicated on drawing)			State of supply Mat.	Supply Std.	Supply Class
STAINLESS STEEL 303					
Title				Scale	
CRYSTAL HOLDER				5:1	
Drawing code				Format	
5.06				A2	
Weight (Kg)				Nr. of sheets	
				001	
Revision				Sheet	Follow
				001	001




ALL DIMENSIONS ARE IN INCHES

TOLERANCES UNLESS OTHERWISE SPECIFIED:
 X.X ± .030
 X.XX ± .010
 X.XXX ± .005

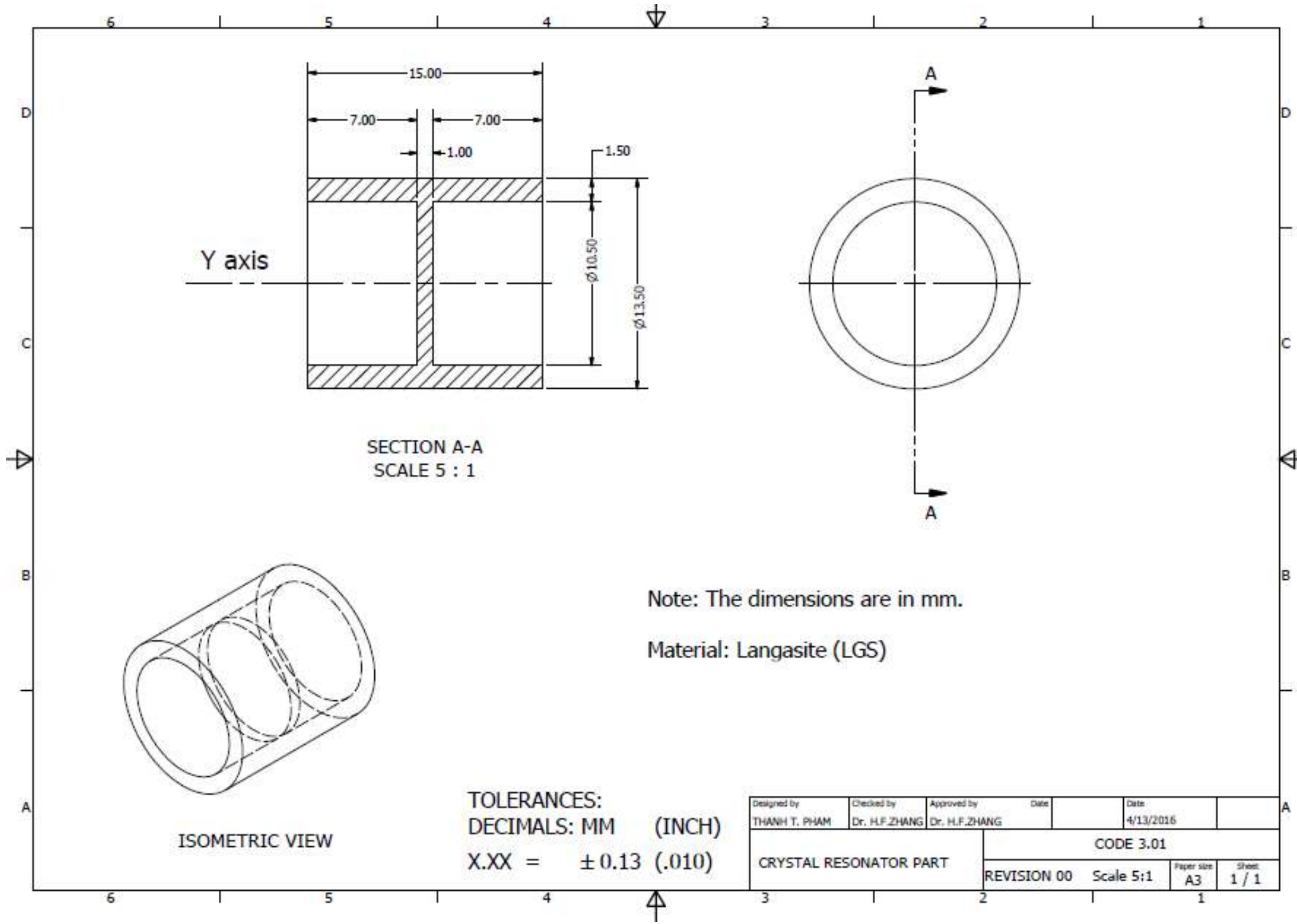
ANGLE: CHAMFER = ±5°

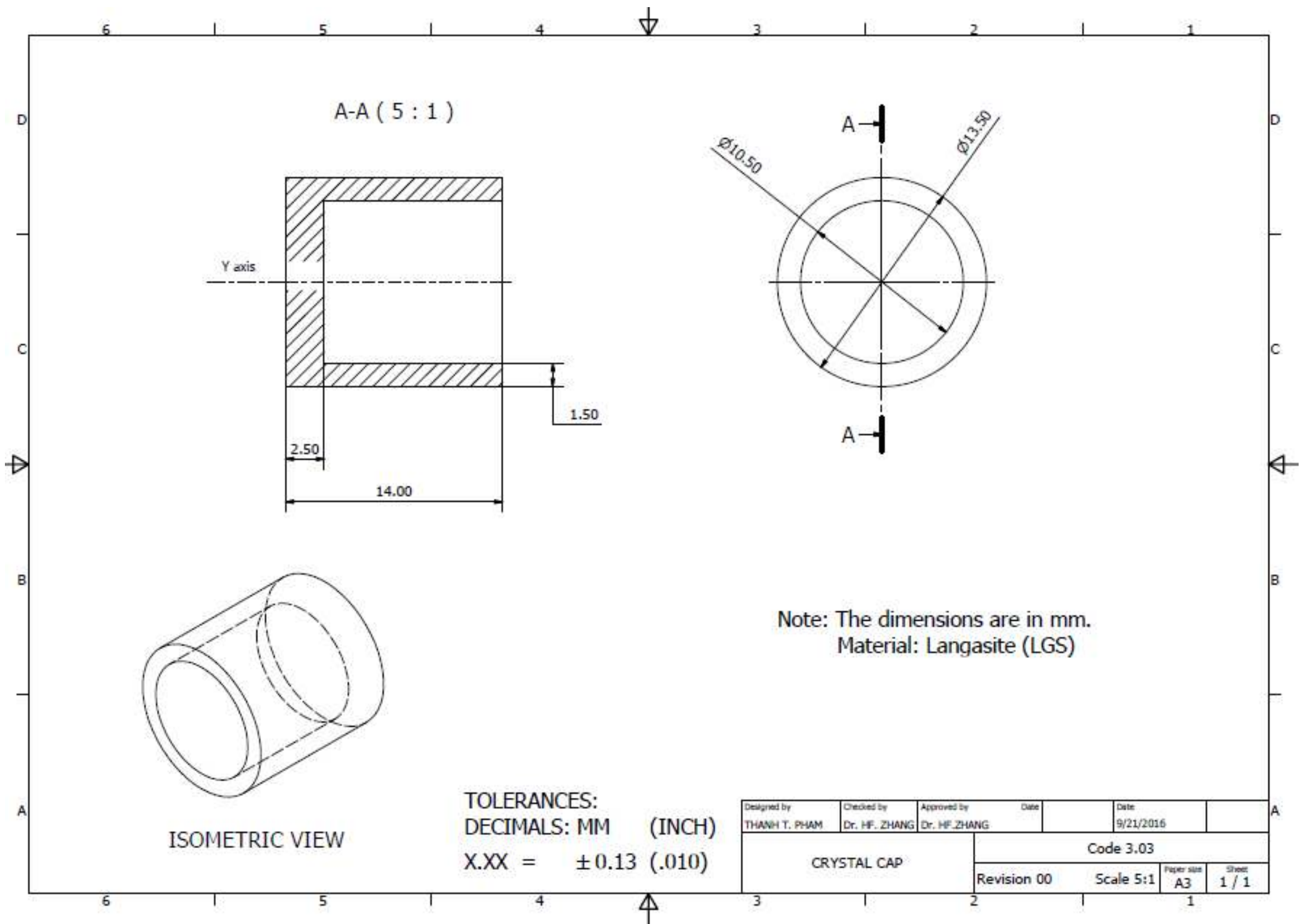
REMOVE ALL BURRS AND SHAPE EDGES
 .005R OR CHAMFER MAX

UNIVERSITY OF NORTH TEXAS, ETEC					
Project name					
PRESSURE SENSOR					
Rev.	Date	Revisions description	Drawn by	Checked by	Approved by
00	08/20/16	ISSUED	THANH.T.PHAM	H.F.ZHANG	H.F.ZHANG
Material (where not indicated on drawing)			Supply Class		
STAINLESS STEEL 303					
Title				Scale	
CRYSTAL HOLDER				5:1	
Drawing code				Nr. of sheets	
5.07				001	
Weight (Kg)		Revision			
Sheet		Follow			
001		001			

APPENDIX B

DESIGN DRAWINGS OF ALL-LANGASITE STRUCTURE





REFERENCES

- [1] Quartzdyne, Inc., "Operation manual for Quartzdyne Digital Pressure Transducer," June 2012.
- [2] John R. Vig., "Temperature-Insensitive Dual-Mode Resonant Sensors-A Review," IEEE Sensors Journal, Vol. 1, No. 1, June 2001.
- [3] Zheyao Wang, Huizhong Zhu, Yonggui Dong and Guanping Feng, " A thickness –Shear Quartz Resonator Force Sensor With Dual-Mode Temperature Compensation," IEEE Sensors Journal, Vol.3, No.4, August 2003.
- [4] F. Della Lucia, P. Zambrozi Jr., F. Frazatto, M. Piazzetta, A. Gobbi, "Design, fabrication and characterization of SAW pressure sensors for offshore oil and gas exploration," Elsevier B.V. 2014.
- [5] Haifeng Zhang, Benjamin D. Montz, Tinghui Fan and John A. Kosinski, "Wireless Langasite Resonator as a Force Sensor," IEEE 2012.
- [6] Roger W. Ward & Robert B. Wiggins, "Quartz pressure transducer technologies," Quartzdyne, Inc, May 1997.
- [7] Quartzdyne, Inc., "Transient performance of Quartzdyne pressure transducers," March 2003.
- [8] Errol P. EerNisse, Robert B. Wiggins, "Review of Thickness-Shear Mode Quartz Resonator Sensors for Temperature and Pressure," IEEE sensors journal, June 2001.
- [9] Errol P. EerNisse, "Quartz resonators vs their environment: Time base or sensor?," The Japan society of applied Physics, 2001.

- [10] H. Edward, Jerry Leach, "A quartz resonator pressure transducer," IEEE transactions on industrial electronics and control instrumentation, Vol. IECI-16, No. 1. July 1969.
- [11] R.J. Besson, J.J. Boy, B. Glotin, Y. Jinzaki, Bikash Sinha, M. Valdois, "A dual-mode thickness-shear quartz pressure sensor," IEEE transaction on ultrasonics, ferroelectrics, and frequency control, vol.40, No. 5, September 1993.
- [12] Yu-Ching Lin, Ayumi Asakura, Toshio Fukuda, Fumihito Arai, "Design and fabrication of miniaturized force sensor with quartz crystal resonators," Proceedings of the IEEE/RSJ, November 2007.
- [13] Ayumi Asakura, Toshio Fukuda, Fumihito Arai, "Design, fabrication and characterization of compact force sensor using AT-cut quartz crystal resonators," IEEE/RSJ international conference, September 2008.
- [14] Keisuke Narumi, Toshio Fukuda Fumihito Arai, "Miniaturization and resolution improvement of load sensor using AT-cut quartz crystal resonator," IEEE SI International 2009.
- [15] F. Della Lucia, P. Zambrozi Jr., F. Frazatto, M. Piazzetta, A. Gobbi, "Design, fabrication and characterization of SAW pressure sensors for offshore oil and gas exploration," Elsevier B.V. 2014.
- [16] P. Dineva et al., "Dynamic Fracture of Piezoelectric Materials, Solid Mechanics and Its Applications," Springer International Publishing Switzerland 2014.
- [17] David Salt, "Hy-Q handbook of quartz crystal devices," Van Nostrand Reinhold (UK) Co. Ltd, 1987.

- [18] Hewlett Packard company "Fundamentals of quartz oscillators, application note 200-2," May 1997.
- [19] Mihir S. Patel, Bikash K. Sinha, "Stress and temperature compensated orientations for thickness shear langasite resonators for high temperature and high pressure environment," IEEE transactions on ultrasonics, ferroelectrics, and frequency control, vol. 62, no. 6, June 2015.
- [20] H. Zhang, J. A. Turner, J. S. Yang, and J. A. Kosinski, "Force-frequency effect of thickness mode langasite resonators," Ultrasonics, 50, pp.479-490, 2010.
- [21] John R. Vig, "Introduction to Quartz frequency standards," Research and development technical report SLCET-TR-92-1 (Rev.1), Army research laboratory, October 1992.
- [22] C. Barthod, "New force sensor based on a double ended tuning fork," in Proc. IEEE Int. Frequency Control Symp., pp. 74-78, 2000.
- [23] J. M. Ratajski, "Force-frequency coefficient of singly rotated vibrating quartz crystals," IBM J. Res. Dev., vol. 12, no. 1, pp. 92-99, 1968.
- [24] A. Ballato, E. P. EerNisse, and T. Lukaszek, "The force-frequency effect in doubly rotated quartz resonators," in Proc. IEEE Int. Frequency Control Symp., pp. 8-16, 1977.
- [25] E. P. EerNisse, "Temperature dependence of the force frequency effect for the AT-, FC-, SC-, and rotated X-cuts," in Proc. IEEE Ultrasonics Symp., pp. 426-430, 1980.
- [26] J. J. Boy, R. J. Besson, E. Bigler, R. Bourquin, and B. Dulmet, "Theoretical and experimental studies of the force-frequency effect in BAW LGS and LGT resonators," in Proc. IEEE Int. Frequency Control Symp., pp. 223-226, 2001.

- [27] Y. Kim, A. Ballato, Force-frequency effect of Y-cut langanite and Y-cut langatate," IEEE Trans. Ultrason. Ferroelectr. Freq. Control, vol. 50, no. 12, pp. 1678-1682, 2003.
- [28] J. M. Ratajski, "The force sensitivity of AT-cut quartz crystal," 20th Annual Symp. on Freq. Control, pp. 33-49, 1966.
- [29] Thanh Tuong Pham, Haifeng Zhang, "A new apparatus for the measurement of force-frequency effect of crystal resonators," Measurement Journal, Volume 93, pp. 524-528, 2016.
- [30] J. M. Ratajski, "Force-frequency coefficient of singly rotated vibrating quartz crystals," IBM J. Res. Dev., vol. 12, no. 1, pp. 92-99, 1968.
- [31] J. A. Kosinski, R. A. Pastore Jr., X. M. Yang, J. S. Yang, and J. A. Turner, "Stress-induced frequency shifts in langasite thickness-mode resonators," IEEE Transactions on Ultrasonics, Ferroelectrics, and Frequency Control, vol. 56, no. 1, January 2009.
- [32] Irina Mateescu, Jiri Zelenka, Jaroslav Nosek, Gary Johnson, "Frequency-Temperature Characteristics of the Langasite Resonators," IEEE Interational Frequency Control Symposium and PDA Exhibition, 2001.
- [33] Zheyao Wang, Huizhong Zhu, Yonggui Dong and Guanping Feng, "A temperature insensitive quartz resonator force sensor," Meas. Sci. Technol. 11 (2000) 1565-1569, July 2000.
- [34] Zheyao Wang, Huizhong Zhu, Yonggui Dong and Guanping Feng, "Development of a High-Resolution Quartz Resonator Force and Weight Sensor With Increased Reliability," IEEE/ASME Transactions on Mechatronics, Vol. 9, No.2, June 2004.

- [35] Lawrence D. Clayton and Errol P. EerNisse, "Quartz Thickness-Shear Mode Pressure Sensor Designed For Enhanced Sensitivity," IEEE Transactions on Ultrasonics, Ferroelectrics, and Frequency control, Vol. 45, No. 5, Sep. 1998.
- [36] Frische et al, "Vibrating quartz diaphragm pressure sensor," Patent 4,479,070, Oct. 23, 1984.
- [37] Marco Ferrari and Vittorio Ferrari, "An oscillator circuit for dual-harmonic tracking of frequency and resistance in quartz resonator sensor," Measurement science and technology 20 (2009) 124005 (11pp).